Computation of the dynamic scalar response of large two-dimensional periodic and symmetric structures by the wave finite element method

D. Duhamel

Computation of the dynamic scalar response of large two-dimensional periodic and symmetric structures by the wave finite element method

D. Duhamel[a,*]

[a]*Ecole des Ponts ParisTech, Laboratoire Navier, ENPC/UGE/CNRS, 6 et 8 Avenue Blaise Pascal, Cité Descartes, Champs-sur-Marne, 77455 Marne La Vallée Cedex 2, France*

Abstract

In the past, the study of periodic media mainly focused on one-dimensional periodic structures (meaning periodic along one direction), on the one hand to determine the dispersion curves linking the frequencies to the wavenumbers and on the other hand to obtain the response of a structure to an external excitation, both for bounded or unbounded structures. In the latter case, effective approaches have been obtained, based on methods such as the Wave Finite Element (WFE). Two-dimensional periodic media are more complex to analyse but dispersion curves can be obtained rather easily as in the one-dimensional case. Obtaining the steady state response of two-dimensional periodic structures to time-harmonic excitations is much more difficult than for one-dimensional media and the results mainly concern infinite media. This work is about this last case of the steady state response of finite two-dimensional periodic structures to time-harmonic excitations by limiting oneself to structures described by a scalar variable (acoustic, thermal, membrane behaviour) and having symmetries compared to two orthogonal planes parallel to the edges of a substructure. Using the WFE for a rectangular substructure and imposing the wavenumber in one direction, we can numerically calculate the wavenumbers and mode shapes associated with propagation in the perpendicular direction. By building solutions with null forces on parallel boundaries, we can decouple the waves in the two directions parallel to the sides of the rectangle. The solution of each of these two problems is obtained by a fast Fourier transformation giving the amplitudes associated with the waves. By summing the contributions of all these waves we obtain the global solution for a two-dimensional periodic medium with a large number of substructures and a low computing time. Examples are given for the case of a two-dimensional membrane with many substructures and different types of heterogeneities.

Keywords: periodic structures, two-dimensional, wave finite element, scalar equation, finite domain.

1. Introduction

Periodic media have received great attention in the past thanks to their great presence in industry due to the ease of realization of such structures and their physical properties such as the possibility of stopping the propagation of waves for frequencies located in forbidden bands. The most frequent cases relate to one-dimensional periodic media (periodic in one direction) but there are also frequently two-dimensional periodic media (periodic in two directions). For one-dimensional media, the Wave Finite Element (WFE) such as described in [1–14] is a good numerical tool for calculating dispersion curves and the response of these structures to external excitations. The first studies of two-dimensional periodic structures were made by for instance [15] who considered wave propagation in one, two and three-dimensional periodic structures to compute dispersion relations using finite element models. One

*Corresponding author
Email address: denis.duhamel@enpc.fr (D. Duhamel)

can also find the work of [16] who set the two-dimensional equation for computing dispersion relations by focusing on the correct treatment of the balance of forces in the corners. More recently [17] considered two-dimensional wave propagation in periodic lattices made of beams mainly to compute dispersion curves and pass and stop bands. They also showed that the low frequency behaviour could be obtained from effective media theories. Wave propagation in more general two-dimensional periodic structures was considered by [18] who used the wave finite element method to compute dispersion relations. Sandwich plates and cylinders were considered for example as well as viscoelastic material by modelling simple substructures made of a single four nodes element. To improve the computation of dispersion relations for doubly periodic structures, a reduced model obtained by the Craig-Bampton method was used first in [19] for computing the frequencies for given wavenumbers in the case of beam grids, then in [20] for computing the wavenumbers for given frequencies in the case of more complex elastic structures and in [21] who considered the case of non classical damping using a state-space approach with reduced matrices. In [22–25] the reduction of the boundary degrees of freedom was considered in addition while [26] projected the mass and stiffness matrices on a reduced set of Bloch modes. Otherwise [27] used exact wave-based approach to study two-dimensional periodic lattices made of beams for computing dispersion curves. Mechanical systems incorporating damping were considered by [28] to compute dispersion relations while [29] studied the propagation of waves in two-dimensional periodic highly anisotropic textiles by WFE focusing on reduction models to compute dispersion relations and effective properties. Similarly [30] considered wave propagation in plate homogeneous in two-dimensions but with a laminated structure in the thickness using the wave finite element method to compute dispersion relations. The mathematically more complicated case of helical periodic structures was studied by [31] for a simple helical spring and by [32, 33] for double helical structures to compute dispersion relations or force transmissibilities. In these last cases one studies the one-dimensional propagation along the axis of the helix. Two-dimensional wave propagation was considered by [34] for the computation of phononic crystals using wavelet and the boundary element method. Structures with even more complex glide, screw and rotational symmetries are also considered by [35, 36]. In all cases, the purpose for two-dimensional wave propagation was to efficiently calculate the dispersion curves for different structures.

One can also be interested by obtaining the response of such structures to an external excitation. For instance, the computation of infinite doubly periodic structures for harmonic electromagnetic fields was considered by [37] using hybrid Finite Element/Boundary Integral and periodic Green's functions computed with acceleration techniques for a rapid convergence of the series representing the Green's function. One can also find [38] who computed the forced response of infinite two-dimensional periodic media using WFE while [39] focused on homogeneous media still using WFE but with a contour integration to improve the computation of some integrals giving the force response. In [40] two-dimensional phononic crystals under a point force were considered. The medium is finite in one direction and infinite in the other direction. Finite element is used in the finite direction leading to a super cell whereas Fourier series and contour integration for the inverse Fourier transform is used along the infinite direction. Similarly, [41, 42] computed the response of two-dimensional finite and infinite periodic structures to point harmonic and impulsive forces. For finite structures, he found the solution by a modal summation of modes with periodic boundary conditions and then extended the solution to infinite structures for points far enough from the load. Contour integrals and the method of steepest descent were used to simplify the integrals giving the response and this was mainly applied to simple two-dimensional point mass systems. In [43] finite element models were used to compute dispersion curves together with reflected and transmitted wave fields between an homogeneous half-plane and a semi-infinite phononic crystals half-space. The results given by the phononic half-plane modelled with Bloch waves show very good comparison with a full finite element model of a finite phononic domain surrounded with absorbing boundaries made of periodic substructures with increasing damping. Finally, [44] was interested by the homogenization of double

periodic arrays of inclusions with elastostatic behaviour to find effective elastic properties and so also considered infinite media. All these studies are therefore mainly concentrated on the response of infinite or semi-infinite media.

However usual structures are finite and one should be able to obtain the response of finite two-dimensional periodic structures to an external excitation. For instance, [45] experimentally tested the seismic isolation of two-dimensional periodic foundations and found interesting isolation effects for frequencies band gaps even if the number of substructures in the periodic medium was small. Comparisons with full Abaqus computations were done showing similar trends to the experimental results. Note that the calculation on a finite number of substructures can reproduce that of an infinite structure only if special absorbing conditions are introduced on the boundaries of the finite structure. Furthermore, while the band gap effect can be observed with a limited number of substructures, the precise calculation of the response of the structure to an external load requires a more detailed calculation and consideration of the correct number of substructures making up the structure. Infinite dielectric photonics crystals were studied by [46] using the finite element for computing band structure and transmission coefficients of fully periodic or periodic with a defect of finite clusters of substructures by full finite element modelling. In [47] the acoustic radiation of two-dimensional nearly periodic metamaterial plates was computed with 6×6 substructures by the finite element method with the Craig-Bampton reduction and interpolation strategies to reduce the computational cost. Reduction methods were also used for instance by [48] who computed two-dimensional periodic metamaterial structures using interior DoFs reduction by the Craig-Bampton method and an interface DoFs reduction. In [49] an approximate solution built from a linear superposition of waves was used to compute finite two-dimensional periodic structures upto 30x30 cells. More generally, [50] considered various reduction strategies for finite element modelling to compute finite periodic structures. Although the computation of finite two-dimensional structures was considered by these authors, the number of substructures was limited to a few hundreds. So for finite media, few results and effective methods are available if we want to get the "exact" solution as the FEM modelling of the whole structure would get for a large periodic structure. Using the usual finite element method quickly leads to very heavy calculations. A possible approach would be to use one of the many methods that can be found to improve the behavior of the finite element method by attempting to reduce the number of degrees of freedom necessary for the solution of complex problems. For example, in the partition of unity finite element method described in [51–56], functions closer to analytical solutions, for example exponentials, are added to traditional finite element polynomial functions. These are general methods which improve the resolution but nevertheless remain limited in the size of the problems which can be solved, for example because of conditioning problems of the matrices of the systems to be solved. On another side, one can also find many approximate solutions, often for the high frequency range. For instance ray tracing or Statistical Energy Analysis (SEA) can provide estimate of the solution or its power density distribution. This can also be mixed to improve the accuracy as in the Dynamic Energy Analysis as in [57–59]. The precision of the results obtained is, however, not easy to estimate. In our approach, we wish to obtain a result of the same precision as that which a complete finite element calculation would allow.

In this paper, we consider the calculation of a finite periodic medium made up of a large number of substructures under external excitations. The choice which is made in this article is to propose an exact method in the sense that the finite element method can be described as exact. In its current form, the proposed method is limited to media described by a scalar equation such as during the propagation of acoustic waves or vibrations of membranes and having symmetries compared to two orthogonal planes parallel to the edges of a substructure. The method proposed in this article will be based on the WFE and will use as a starting point the mass, stiffness and damping matrices of a finite element model of a rectangular substructure of the periodic medium. By imposing the wavenumber in one direction, we can numerically calculate the wavenumbers and mode shapes associated with

propagation in the perpendicular direction. We can thus build a set of waves propagating respectively along the two directions parallel to the sides of the rectangle which will serve as the basis on which we will decompose the solution. By taking appropriately chosen solutions, thanks to the hypotheses of a scalar equation and symmetries with respect to the sides of the substructure, we can decouple the waves in the two directions parallel to the sides of the rectangle. The solution of each of these two problems is obtained by a fast Fourier transformation which gives the amplitudes associated with the waves. We can then calculate the global solution at selected points by summing the contributions of all these waves. We thus obtain the global solution for a two-dimensional periodic medium with a large number of substructures with a low computing time.

The paper is organised as follows. In section 2, two-dimensional wave modes for periodic media are computed and the decomposition of a two-dimensional problem into two one-dimensional problems is described. In section 3, special symmetric solutions are computed which allows to set the equations of the global problem in section 4. These equations are solved in section 5 while section 6 presents some numerical results for the case of a two-dimensional membrane with holes or many heterogeneous inclusions before the conclusion in section 7.

2. Two-dimensional wave modes

2.1. Relations on boundary variables

In the aim of building wave modes, we first concentrate on the behaviour of a substructure. The discrete dynamic equation of a substructure (an elementary period) obtained from a finite element (FE) model at a circular frequency ω and for the time dependence $e^{i\omega t}$ is given by:

$$((1+\xi i)\mathbf{K} - \omega^2\mathbf{M})\tilde{\mathbf{q}} = \tilde{\mathbf{f}} \tag{1}$$

where $\mathbf{K}$ and $\mathbf{M}$ are the stiffness and mass matrices, respectively, ξ is the damping coefficient, $\tilde{\mathbf{f}}$ is the loading vector and $\tilde{\mathbf{q}}$ the vector of the degrees of freedom (DoFs). Other forms of damping, such as viscous damping, would be possible as long as a dynamic stiffness matrix is obtained in the frequency domain. Introducing the dynamic stiffness matrix $\widetilde{\mathbf{D}} = (1+\xi i)\mathbf{K} - \omega^2\mathbf{M}$, decomposing the DoFs into boundary (b) and interior (i) DoFs, and assuming that there are no external forces on the interior nodes, result in the following equation:

$$\begin{bmatrix} \widetilde{\mathbf{D}}_{bb} & \widetilde{\mathbf{D}}_{bi} \\ \widetilde{\mathbf{D}}_{ib} & \widetilde{\mathbf{D}}_{ii} \end{bmatrix} \begin{bmatrix} \tilde{\mathbf{q}}_b \\ \tilde{\mathbf{q}}_i \end{bmatrix} = \begin{bmatrix} \tilde{\mathbf{f}}_b \\ \mathbf{0} \end{bmatrix} \tag{2}$$

The interior DoFs can be eliminated using the second row of equation (2), which results in

$$\tilde{\mathbf{q}}_i = -\widetilde{\mathbf{D}}_{ii}^{-1}\widetilde{\mathbf{D}}_{ib}\tilde{\mathbf{q}}_b \tag{3}$$

The first row of equation (2) becomes

$$\tilde{\mathbf{f}}_b = \left(\widetilde{\mathbf{D}}_{bb} - \widetilde{\mathbf{D}}_{bi}\widetilde{\mathbf{D}}_{ii}^{-1}\widetilde{\mathbf{D}}_{ib}\right)\tilde{\mathbf{q}}_b \tag{4}$$

which can be written as

$$\tilde{\mathbf{f}}_b = \tilde{\mathbf{D}}_b\tilde{\mathbf{q}}_b \tag{5}$$

or, by dropping the b index and $\tilde{}$, in a more simplified form used in the following

$$\mathbf{f} = \mathbf{D}\mathbf{q} \tag{6}$$

It should be noted that only boundary DoFs are considered in the following. The sizes of vectors $\mathbf{q}$ and $\mathbf{f}$ equals $n_b \times 1$ and $\mathbf{D}$ is a matrix of size $n_b \times n_b$ with n_b the number of DoFs on the boundary of a substructure.

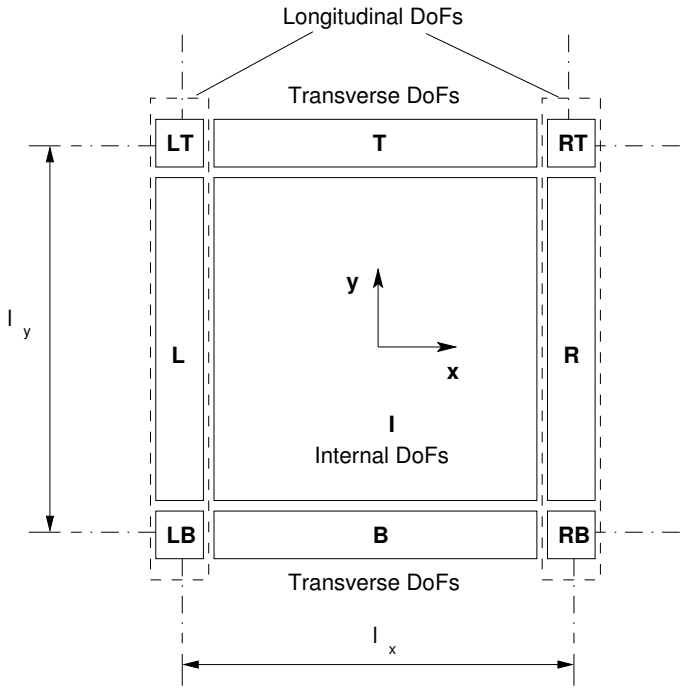

Figure 1: A substructure in the periodic medium

2.2. Condensation of transverse degrees of freedom

The periodic cell is assumed to be meshed with an equal number of nodes on their opposite sides. The boundary DoFs are decomposed into left (L), right (R), bottom (B), top (T) DoFs and associated corners (LB), (RB), (LT) and (RT) as shown in figure 1. The global vector of boundary DoFs of size $n_b \times 1$ is defined as

$$\mathbf{q} = \begin{pmatrix} \mathbf{q}_{LB} \\ \mathbf{q}_{L} \\ \mathbf{q}_{LT} \\ \mathbf{q}_{RB} \\ \mathbf{q}_{R} \\ \mathbf{q}_{RT} \\ \mathbf{q}_{B} \\ \mathbf{q}_{T} \end{pmatrix} \tag{7}$$

Note that $n_b = 4n_{LB} + 2n_L + 2n_B$ with n_{LB} the number of DoFs at a corner (the same for the four corners), n_L the number of DoFs at the left boundary without its corners DoFs and n_B the number of DoFs at the bottom boundary without its corners DoFs. The proposed approach consists first of eliminating the DoFs of the lower and upper sides then of expressing all remaining DoFs from a reduced number of DoFs for which an eigenvalue problem will be posed (see for example [18, 30] for a similar procedure where the problem is set on a reduced number of DoFs). First, the longitudinal DoFs vector is defined as ${}^t\mathbf{q}_l = \begin{bmatrix} {}^t\mathbf{q}_{LB} & {}^t\mathbf{q}_{L} & {}^t\mathbf{q}_{LT} & {}^t\mathbf{q}_{RB} & {}^t\mathbf{q}_{R} & {}^t\mathbf{q}_{RT} \end{bmatrix}$ and its size is $n_l^y = 4n_{LB} + 2n_L$. Thus, equation (6) is rewritten as

$$\begin{bmatrix} \mathbf{D}_{ll} & \mathbf{D}_{lB} & \mathbf{D}_{lT} \\ \mathbf{D}_{Bl} & \mathbf{D}_{BB} & \mathbf{D}_{BT} \\ \mathbf{D}_{Tl} & \mathbf{D}_{TB} & \mathbf{D}_{TT} \end{bmatrix} \begin{bmatrix} \mathbf{q}_l \\ \mathbf{q}_B \\ \mathbf{q}_T \end{bmatrix} = \begin{bmatrix} \mathbf{f}_l \\ \mathbf{f}_B \\ \mathbf{f}_T \end{bmatrix} \tag{8}$$

We are looking for solutions such that the DoFs at the bottom and top boundaries are connected by a propagation constant λ_y along y and using the effort equilibrium at the bottom side of the cell, relations between the transverse DoFs are given by

$$\begin{array}{rcl} \mathbf{q}_T & = & \lambda_y \mathbf{q}_B \\ \mathbf{f}_B + \frac{1}{\lambda_y}\mathbf{f}_T & = & 0 \end{array} \tag{9}$$

Multiplying the third row of equation (8) with $\frac{1}{\lambda_y}$, taking the sum of the second and third rows of equation (8), using conditions (9), lead to

$$\left(\mathbf{D}_{Bl} + \frac{1}{\lambda_y}\mathbf{D}_{Tl}\right)\mathbf{q}_l + \left(\mathbf{D}_{BB} + \mathbf{D}_{TT} + \frac{1}{\lambda_y}\mathbf{D}_{TB} + \lambda_y \mathbf{D}_{BT}\right)\mathbf{q}_B = 0 \tag{10}$$

so

$$\mathbf{q}_B = -\left(\mathbf{D}_{BB} + \mathbf{D}_{TT} + \frac{1}{\lambda_y}\mathbf{D}_{TB} + \lambda_y \mathbf{D}_{BT}\right)^{-1}\left(\mathbf{D}_{Bl} + \frac{1}{\lambda_y}\mathbf{D}_{Tl}\right)\mathbf{q}_l \tag{11}$$

Using (9) and (11), the first row of equation (8) becomes

$$\begin{array}{rcl} \mathbf{f}_l & = & \left[\mathbf{D}_{ll} - (\mathbf{D}_{lB} + \lambda_y \mathbf{D}_{lT})\left(\mathbf{D}_{BB} + \mathbf{D}_{TT} + \frac{1}{\lambda_y}\mathbf{D}_{TB} + \lambda_y \mathbf{D}_{BT}\right)^{-1}\right. \\ & & \left. \times \left(\mathbf{D}_{Bl} + \frac{1}{\lambda_y}\mathbf{D}_{Tl}\right)\right]\mathbf{q}_l \end{array} \tag{12}$$

which can be written as

$$\mathbf{f}_l = \mathbf{D}_l \mathbf{q}_l \tag{13}$$

The sizes of vectors $\mathbf{q}_l$ and $\mathbf{f}_l$ equals $n_l^y \times 1$ and $\mathbf{D}_l$ is a matrix of size $n_l^y \times n_l^y$ with $n_l^y = 4n_{LB} + 2n_L$. One notices that we have

$$\mathbf{D}_l(\lambda_y) = {}^t\mathbf{D}_l(\frac{1}{\lambda_y}) \tag{14}$$

2.3. One-dimensional eigenvalue problem

Introducing the propagation constants λ_x along x and λ_y along y lead to the following relations between longitudinal DoFs

$$\begin{array}{rcl} \mathbf{q}_R & = & \lambda_x \mathbf{q}_L \\ \mathbf{q}_{RB} & = & \lambda_x \mathbf{q}_{LB} \\ \mathbf{q}_{RT} & = & \lambda_x \lambda_y \mathbf{q}_{LB} \\ \mathbf{q}_{LT} & = & \lambda_y \mathbf{q}_{LB} \end{array} \tag{15}$$

From these conditions (15), it can be seen that all components of the vector $\mathbf{q}_l$ depend on the reduced set of DoFs defined by $\mathbf{q}_r = {}^t\left[{}^t\mathbf{q}_{LB} \quad {}^t\mathbf{q}_L\right]$. This can be expressed as

$$\mathbf{q}_l = \left(\mathbf{W}_0(\lambda_y) + \lambda_x \mathbf{W}_1(\lambda_y)\right)\mathbf{q}_r \tag{16}$$

where the matrices $\mathbf{W}_0(\lambda_y)$ and $\mathbf{W}_1(\lambda_y)$ depend on the propagation constant λ_y and are given by

$$\mathbf{W}_0(\lambda_y) = \begin{bmatrix} \mathbf{I}_{n_{LB}\times n_{LB}} & \mathbf{o}_{n_{LB}\times n_L} \\ \mathbf{o}_{n_L\times n_{LB}} & \mathbf{I}_{n_L\times n_L} \\ \lambda_y \mathbf{I}_{n_{LB}\times n_{LB}} & \mathbf{o}_{n_{LB}L\times n_L} \\ \mathbf{o}_{n_{LB}\times n_{LB}} & \mathbf{o}_{n_{LB}\times n_L} \\ \mathbf{o}_{n_L\times n_{LB}} & \mathbf{o}_{n_L\times n_L} \\ \mathbf{o}_{n_{LB}\times n_{LB}} & \mathbf{o}_{n_{LB}\times n_L} \end{bmatrix} \qquad \mathbf{W}_1(\lambda_y) = \begin{bmatrix} \mathbf{o}_{n_{LB}\times n_{LB}} & \mathbf{o}_{n_{LB}\times n_L} \\ \mathbf{o}_{n_L\times n_{LB}} & \mathbf{o}_{n_L\times n_L} \\ \mathbf{o}_{n_{LB}\times n_{LB}} & \mathbf{o}_{n_{LB}\times n_L} \\ \mathbf{I}_{n_{LB}\times n_{LB}} & \mathbf{o}_{n_{LB}\times n_L} \\ \mathbf{o}_{n_L\times n_{LB}} & \mathbf{I}_{n_L\times n_L} \\ \lambda_y \mathbf{I}_{n_{LB}\times n_{LB}} & \mathbf{o}_{n_{LB}\times n_L} \end{bmatrix} \tag{17}$$

with $\mathbf{I}$ the identity matrix and $\mathbf{o}$ the null matrix. Note that the size of vector $\mathbf{q}_r$ equals $n_r^y \times 1$ with $n_r^y = n_{LB} + n_L$ is the number of DoFs on the left side minus the number of DoFs at the upper left corner and $\mathbf{W}_0$ and $\mathbf{W}_1$ are matrices of size $n_l^y \times n_r^y$. The equilibrium conditions between adjacent cells are given by

$$\begin{array}{rcl} \lambda_x \mathbf{f}_L + \mathbf{f}_R &=& 0 \\ \lambda_x \mathbf{f}_{LB} + \mathbf{f}_{RB} + \frac{\lambda_x}{\lambda_y}\mathbf{f}_{LT} + \frac{1}{\lambda_y}\mathbf{f}_{RT} &=& 0 \end{array} \tag{18}$$

that can be written as

$$\left(\lambda_x {}^t\mathbf{W}_0(\frac{1}{\lambda_y}) + {}^t\mathbf{W}_1(\frac{1}{\lambda_y})\right)\mathbf{f}_l = 0 \tag{19}$$

Combining (13), (16) and (19), lead to

$$\left(\lambda_x {}^t\mathbf{W}_0(\frac{1}{\lambda_y}) + {}^t\mathbf{W}_1(\frac{1}{\lambda_y})\right)\mathbf{D}_l(\lambda_y)\left(\mathbf{W}_0(\lambda_y) + \lambda_x \mathbf{W}_1(\lambda_y)\right)\mathbf{q}_r = 0 \tag{20}$$

that can be written as

$$\left(\mathbf{A}_{RL} + \lambda_x(\mathbf{A}_{LL} + \mathbf{A}_{RR}) + \lambda_x^2 \mathbf{A}_{LR}\right)\mathbf{q}_r = 0 \tag{21}$$

where

$$\begin{array}{rcl} \mathbf{A}_{RL}(\lambda_y) &=& {}^t\mathbf{W}_1(\frac{1}{\lambda_y})\mathbf{D}_l(\lambda_y)\mathbf{W}_0(\lambda_y) \\ \mathbf{A}_{LL}(\lambda_y) &=& {}^t\mathbf{W}_0(\frac{1}{\lambda_y})\mathbf{D}_l(\lambda_y)\mathbf{W}_0(\lambda_y) \\ \mathbf{A}_{RR}(\lambda_y) &=& {}^t\mathbf{W}_1(\frac{1}{\lambda_y})\mathbf{D}_l(\lambda_y)\mathbf{W}_1(\lambda_y) \\ \mathbf{A}_{LR}(\lambda_y) &=& {}^t\mathbf{W}_0(\frac{1}{\lambda_y})\mathbf{D}_l(\lambda_y)\mathbf{W}_1(\lambda_y) \end{array} \tag{22}$$

Note that these four matrices are of sizes $n_r^y \times n_r^y$. One also has from (14) and (22)

$$\begin{array}{rcl} {}^t\mathbf{A}_{RL}(\lambda_y) &=& \mathbf{A}_{LR}(1/\lambda_y) \\ {}^t\mathbf{A}_{LL}(\lambda_y) &=& \mathbf{A}_{LL}(1/\lambda_y) \\ {}^t\mathbf{A}_{RR}(\lambda_y) &=& \mathbf{A}_{RR}(1/\lambda_y) \\ {}^t\mathbf{A}_{LR}(\lambda_y) &=& \mathbf{A}_{RL}(1/\lambda_y) \end{array} \tag{23}$$

Note that if λ_y yields the set of eigenvalues $(\lambda_x^1, \ldots, \lambda_x^{2n_r^y})$ then the set associated to $\frac{1}{\lambda_y}$ is $(\frac{1}{\lambda_x^1}, \ldots, \frac{1}{\lambda_x^{2n_r^y}})$ because one has from (21) and (23)

$$\left({}^t\mathbf{A}_{LR}(\frac{1}{\lambda_y}) + \lambda_x({}^t\mathbf{A}_{LL}(\frac{1}{\lambda_y}) + {}^t\mathbf{A}_{RR}(\frac{1}{\lambda_y})) + \lambda_x^2 {}^t\mathbf{A}_{RL}(\frac{1}{\lambda_y})\right)\mathbf{q}_r(\lambda_y) = 0 \tag{24}$$

or

$${}^t\mathbf{q}_r(\lambda_y)\left(\mathbf{A}_{RL}(\frac{1}{\lambda_y}) + \frac{1}{\lambda_x}(\mathbf{A}_{LL}(\frac{1}{\lambda_y}) + \mathbf{A}_{RR}(\frac{1}{\lambda_y})) + \frac{1}{\lambda_x^2}\mathbf{A}_{LR}(\frac{1}{\lambda_y})\right) = 0 \tag{25}$$

and the system and its transpose have the same right and left eigenvalues with possibly different eigenvectors.

As we have taken a small damping, we always have $|\lambda_x| \neq 1$ and the right-going solutions must have a decreasing amplitude as we move on the right, meaning that

$$|\lambda_x^+| < 1 \tag{26}$$

The left going waves are such that

$$|\lambda_x^-| > 1 \tag{27}$$

This allows to define the eigensolutions

$$\begin{array}{lll}
\mathbf{\Lambda}^+(\lambda_y) & = [\lambda^+_{\mathtt{x}1}(\lambda_y) \cdots \lambda^+_{\mathtt{x}J_n^+}(\lambda_y)] & , \quad \mathbf{\Lambda}^-(\lambda_y) = [\lambda^-_{\mathtt{x}1}(\lambda_y) \cdots \lambda^-_{\mathtt{x}J_n^-}(\lambda_y)] \\
\mathbf{\Phi}^+_{\mathtt{q}}(\lambda_y) & = [\boldsymbol{\phi}^+_{\mathtt{q}1}(\lambda_y) \cdots \boldsymbol{\phi}^+_{\mathtt{q}J_n^+}(\lambda_y)] & , \quad \mathbf{\Phi}^-_{\mathtt{q}}(\lambda_y) = [\boldsymbol{\phi}^-_{\mathtt{q}1}(\lambda_y) \cdots \boldsymbol{\phi}^-_{\mathtt{q}J_n^-}(\lambda_y)] \\
\mathbf{\Phi}^+_{\mathtt{F}}(\lambda_y) & = [\boldsymbol{\phi}^+_{\mathtt{F}1}(\lambda_y) \cdots \boldsymbol{\phi}^+_{\mathtt{F}J_n^+}(\lambda_y)] & , \quad \mathbf{\Phi}^-_{\mathtt{F}}(\lambda_y) = [\boldsymbol{\phi}^-_{\mathtt{F}1}(\lambda_y) \cdots \boldsymbol{\phi}^-_{\mathtt{F}J_n^-}(\lambda_y)].
\end{array} \tag{28}$$

in which $\boldsymbol{\phi}_{\mathtt{qj}}$ is the solution of the eigenproblem (21) and $\boldsymbol{\phi}_{\mathtt{Fj}} = {}^t\begin{bmatrix} {}^t\mathbf{f}^j_{LB} & {}^t\mathbf{f}^j_{L} \end{bmatrix}$ the associated force vector. Note that J_n^+ is the number of right-going waves and J_n^- is the number of left-going waves such that $J_n^+ + J_n^- = 2n_r^y = 2(n_{LB} + n_L)$ which equals two times the size of the eigenproblem (21).

2.4. Behaviour at corners

Consider for instance the LB corner. The force $\mathbf{F}_{LB}$ at this corner is made of a force $\mathbf{F}^x_{LB}$ coming from the bottom boundary and a part $\mathbf{F}^y_{LB}$ coming from the left boundary so that we can write

$$\mathbf{F}_{LB} = \mathbf{F}^x_{LB} + \mathbf{F}^y_{LB} \tag{29}$$

One knows the value of $\mathbf{F}_{LB}$ from relation (13) but the values of $\mathbf{F}^x_{LB}$ and $\mathbf{F}^y_{LB}$ are unknown. In the same way, one has

$$\begin{array}{lll}
\mathbf{F}_{LT} & = & \mathbf{F}^x_{LT} + \mathbf{F}^y_{LT} \\
\mathbf{F}_{RB} & = & \mathbf{F}^x_{RB} + \mathbf{F}^y_{RB} \\
\mathbf{F}_{RT} & = & \mathbf{F}^x_{RT} + \mathbf{F}^y_{RT}
\end{array} \tag{30}$$

The horizontal and vertical parts of the forces satisfy the following relations

$$\begin{array}{lll}
\mathbf{F}^x_{LB} + \dfrac{1}{\lambda_y}\mathbf{F}^x_{LT} & = & 0 \\
\mathbf{F}^y_{LB} + \dfrac{1}{\lambda_x}\mathbf{F}^y_{RB} & = & 0 \\
\mathbf{F}^x_{RB} + \dfrac{1}{\lambda_y}\mathbf{F}^x_{RT} & = & 0 \\
\mathbf{F}^y_{LT} + \dfrac{1}{\lambda_x}\mathbf{F}^y_{RT} & = & 0
\end{array} \tag{31}$$

From relations (29), (30) and (31) one can eliminate the x parts to get

$$\begin{array}{lll}
\mathbf{F}_{LB} + \dfrac{1}{\lambda_y}\mathbf{F}_{LT} & = & \mathbf{F}^y_{LB} + \dfrac{1}{\lambda_y}\mathbf{F}^y_{LT} \\
\mathbf{F}_{RB} + \dfrac{1}{\lambda_y}\mathbf{F}_{RT} & = & \mathbf{F}^y_{RB} + \dfrac{1}{\lambda_y}\mathbf{F}^y_{RT} \\
\mathbf{F}^y_{LB} + \dfrac{1}{\lambda_x}\mathbf{F}^y_{RB} & = & 0 \\
\mathbf{F}^y_{LT} + \dfrac{1}{\lambda_x}\mathbf{F}^y_{RT} & = & 0
\end{array} \tag{32}$$

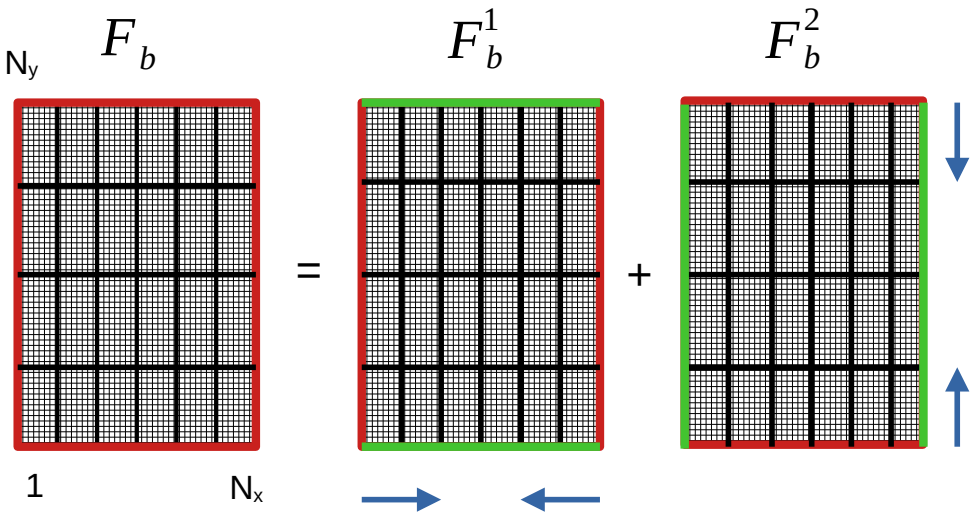

Figure 2: Decomposition of boundary loads into two side loads: loaded boundary in red, free boundary in green.

This is an indeterminate system because adding the first line to the second line multiplied by $1/\lambda_x$ should yield zero according to relation (18). So the first and second relations are not independent and it is not possible to obtain the exact values of the x and y parts of the force from these relations. However, we will propose an approximate method which seems to give good numerical results and which improves the precision of the solutions. The solutions we obtain are waves that can be approximated by shapes like $e^{i(k_x x+k_y y)}$ (that would be accurate if the medium were homogeneous). The F^y part should be approximately the x derivative and given by $F^y \approx ik_x e^{i(k_x x+k_y y)}$ and one has $\mathbf{F}^y_{LB} \simeq \frac{1}{\lambda_y}\mathbf{F}^y_{LT}$ if $\lambda_y \approx e^{ik_y l_y}$. So we get the estimate at the corners

$$\begin{aligned} \mathbf{F}^y_{LB} &\simeq \frac{1}{2}(\mathbf{F}_{LB} + \frac{1}{\lambda_y}\mathbf{F}_{LT}) \\ \mathbf{F}^y_{LT} &\simeq \frac{\lambda_y}{2}(\mathbf{F}_{LB} + \frac{1}{\lambda_y}\mathbf{F}_{LT}) \end{aligned} \tag{33}$$

Finally, for the problem considered at section 2.3, where we are looking for waves in the x direction, one choose to only keep the y parts of the force at corners, as given by (33), for the force vector in relation (28). These components are linked by the propagation constants λ_y along y and λ_x along x. The same thing is done for all force vectors with a component associated with a corner.

2.5. Reduction to one-dimensional problems

Consider now a rectangular domain made of $N_x \times N_y$ substructures and which undergoes forces over its left/right and bottom/top edges, as depicted in Figure 2 where the loads are shown as red lines on the boundary while free sides are depicted as green lines. The global loads can be decomposed as loads on the vertical sides $\mathbf{F}^1_b$ and loads on the horizontal sides $\mathbf{F}^2_b$ such that the displacements of the global problem can be recovered as the sum of the displacements of problems 1 and 2. So we have

$$\mathbf{F}_b = (\mathbf{F}_b)^1 + (\mathbf{F}_b)^2 \quad \Rightarrow \quad \mathbf{q}_b = (\mathbf{q}_b)^1 + (\mathbf{q}_b)^2. \tag{34}$$

The key idea behind the present approach is to decompose the vector of forces $\mathbf{F}_b$ into two states of excitation $(\mathbf{F}_b)^1$ and $(\mathbf{F}_b)^2$ that operate, respectively, on the vertical and horizontal edges (see Figure

2). The solution is then expressed in terms of wave modes traveling along both horizontal and vertical directions, as shown in Figure 2.

We focus now on one of the two problems defined before. Consider for instance the first problem as the second problem can be solved in the same way. From the knowledge of the propagation constants and wave modes for one-dimensional WFE, the vectors of displacements and forces of an assembly of N_x substructures like the one displayed in Figure 2 are expressed on global left ($\overline{L}$) and right ($\overline{R}$) boundaries in terms of wave shapes, as follows:

$$\begin{aligned} \mathbf{q}_{\overline{L}} &= \mathbf{\Phi}_{\mathtt{q}}\mathbf{Q} + \mathbf{\Phi}^{\star}_{\mathtt{q}}\boldsymbol{\mu}^{N_x}\mathbf{Q}^{\star}, \quad -\mathbf{F}_{\overline{L}} &= \mathbf{\Phi}_{\mathtt{F}}\mathbf{Q} + \mathbf{\Phi}^{\star}_{\mathtt{F}}\boldsymbol{\mu}^{N_x}\mathbf{Q}^{\star} \\ \mathbf{q}_{\overline{R}} &= \mathbf{\Phi}_{\mathtt{q}}\boldsymbol{\mu}^{N_x}\mathbf{Q} + \mathbf{\Phi}^{\star}_{\mathtt{q}}\mathbf{Q}^{\star}, \quad \mathbf{F}_{\overline{R}} &= \mathbf{\Phi}_{\mathtt{F}}\boldsymbol{\mu}^{N_x}\mathbf{Q} + \mathbf{\Phi}^{\star}_{\mathtt{F}}\mathbf{Q}^{\star} \end{aligned} \tag{35}$$

where $\mathbf{Q}$ and $\mathbf{Q}^{\star}$ are vectors of wave amplitudes which are respectively defined at the left and right edges of the whole domain, i.e., at the substructure boundaries (1) and (N_x+1). The elements of the diagonal matrix $\boldsymbol{\mu}$ have modulus less or equal to one.

The problem behind the computation of the forced response can be stated as to find the vectors of wave amplitudes $\mathbf{Q}$ and $\mathbf{Q}^{\star}$. This is achieved by considering the boundary conditions (BCs) on the left and right edges, the other structure boundaries being assumed to be free from excitations sources (see Figure 2). Those BCs may involve prescribed forces/moments $\mathbf{F}_0$ and $\mathbf{F}^{\star}_0$ that apply over the substructure boundaries 1 and N_x+1, respectively, as shown in Figure 2. The related wave expansion, Eq. (35), yields

$$-\mathbf{F}_0 = \mathbf{\Phi}_{\mathtt{F}}\mathbf{Q} + \mathbf{\Phi}^{\star}_{\mathtt{F}}\boldsymbol{\mu}^{N_x}\mathbf{Q}^{\star}, \quad \mathbf{F}^{\star}_0 = \mathbf{\Phi}_{\mathtt{F}}\boldsymbol{\mu}^{N_x}\mathbf{Q} + \mathbf{\Phi}^{\star}_{\mathtt{F}}\mathbf{Q}^{\star}. \tag{36}$$

The problem is to find the wave modes $\mathbf{\Phi}_{\mathtt{F}}$ and $\mathbf{\Phi}^{\star}_{\mathtt{F}}$ with free boundaries (no force on the bottom and top boundaries) and to efficiently solve relation (36). This could be done using the one-dimensional WFE method with wave modes and propagation constants computed from the modelling of a vertical slice with free bottom and top boundaries. However this would not use the periodicity of the slice along the vertical direction. So, in the following a true two-dimensional approach will be used starting from waves computed on only one substructure. Note that the loading is applied only on the boundary of the domain. In the case of a point force which would be applied inside the domain, the loading could be transformed into a loading on the boundary using the Green's function of the periodic domain which can for example be estimated by the techniques developed in [38, 39, 41]. In this article, for simplicity we will limit ourselves to loadings on the boundary of the domain.

3. Building eigenvectors with free boundary

3.1. Symmetric solution

We suppose now that the geometry and mechanical parameters of a period are invariant by substituting $l_y - y$ to y as in figure 3. We also make the hypothesis that the dynamic stiffness matrix is invariant by this transformation. Consider a solution defined by the vectors

$$\begin{bmatrix} \mathbf{q}_l \\ \mathbf{q}_B \\ \mathbf{q}_T \end{bmatrix} \quad and \quad \begin{bmatrix} \mathbf{f}_l \\ \mathbf{f}_B \\ \mathbf{f}_T \end{bmatrix} \tag{37}$$

such that

$$\begin{aligned} \mathbf{q}_T &= \lambda_y \mathbf{q}_B \\ \mathbf{f}_B + \tfrac{1}{\lambda_y}\mathbf{f}_T &= 0 \end{aligned} \tag{38}$$

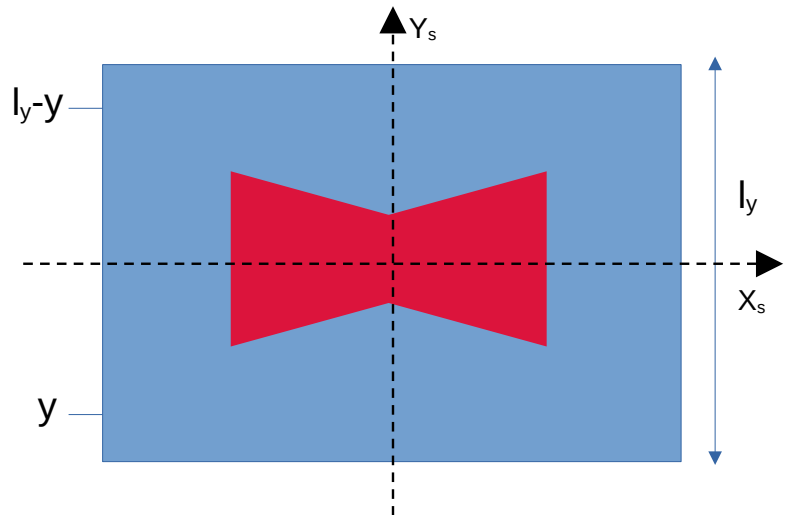

Figure 3: Symmetric cell about the X_x and Y_s axis.

and relation (8), so that

$$\begin{aligned} \mathbf{f}_B &= \mathbf{D}_{Bl}\mathbf{q}_l + (\mathbf{D}_{BB} + \lambda_y \mathbf{D}_{BT})\mathbf{q}_B \\ \mathbf{f}_T &= \mathbf{D}_{Tl}\mathbf{q}_l + (\mathbf{D}_{TB} + \lambda_y \mathbf{D}_{TT})\mathbf{q}_B \end{aligned} \tag{39}$$

Now, denoting $\mathbf{q}(x, y)$ the displacement associated to this solution, one defines the symmetric solution such that

$$\tilde{\mathbf{q}}(x, y) = \mathbf{q}(x, -y) = \frac{1}{\lambda_y}\mathbf{q}(x, l_y - y) \tag{40}$$

So the symmetric solution is such that

$$\tilde{\mathbf{q}}(x, y + l_y) = \mathbf{q}(x, -y - l_y) = \frac{1}{\lambda_y}\mathbf{q}(x, -y) = \frac{1}{\lambda_y}\tilde{\mathbf{q}}(x, y) \tag{41}$$

and

$$\begin{aligned} \tilde{\mathbf{q}}_B &= \mathbf{q}_B \\ \tilde{\mathbf{q}}_T &= \frac{1}{\lambda_y}\tilde{\mathbf{q}}_B = \frac{1}{\lambda_y}\mathbf{q}_B \end{aligned} \tag{42}$$

Concerning the forces associated to the symmetric solution, one has

$$\begin{aligned} \tilde{\mathbf{f}}_B &= \mathbf{D}_{Bl}\tilde{\mathbf{q}}_l + \mathbf{D}_{BB}\tilde{\mathbf{q}}_B + \mathbf{D}_{BT}\tilde{\mathbf{q}}_T \\ \tilde{\mathbf{f}}_T &= \mathbf{D}_{Tl}\tilde{\mathbf{q}}_l + \mathbf{D}_{TB}\tilde{\mathbf{q}}_B + \mathbf{D}_{TT}\tilde{\mathbf{q}}_T \end{aligned} \tag{43}$$

We make the hypothesis that the symmetry of the structure leads to the following relations on the submatrices.

$$\begin{aligned} \mathbf{D}_{BB} &= \mathbf{D}_{TT} \\ \mathbf{D}_{BT} &= \mathbf{D}_{TB} \\ \mathbf{D}_{TB} &= \mathbf{D}_{BT} \\ \mathbf{D}_{TT} &= \mathbf{D}_{BB} \end{aligned} \tag{44}$$

or more generally

$$\mathbf{D}_{ij} = \mathbf{D}_{\tilde{i}\tilde{j}} \tag{45}$$

where $\tilde{i}$ and $\tilde{j}$ are the DoFs at $y_i - l_y$ and $y_j - l_y$ if y_i and y_j are the locations of the DoFs i and j. The longitudinal vector of the symmetric solution is

$$\tilde{\mathbf{q}}_l = \begin{bmatrix} \tilde{\mathbf{q}}_{LB} \\ \tilde{\mathbf{q}}_L \\ \tilde{\mathbf{q}}_{LT} \\ \tilde{\mathbf{q}}_{RB} \\ \tilde{\mathbf{q}}_R \\ \tilde{\mathbf{q}}_{RT} \end{bmatrix} = \frac{1}{\lambda_y} \begin{bmatrix} \mathbf{q}_{LT} \\ \mathbf{q}_{\tilde{L}} \\ \mathbf{q}_{LB} \\ \mathbf{q}_{RT} \\ \mathbf{q}_{\tilde{R}} \\ \mathbf{q}_{RB} \end{bmatrix} = \frac{1}{\lambda_y} \mathbf{q}_{\tilde{l}} \tag{46}$$

where we have denoted $\mathbf{q}_{\tilde{L}}$ and $\mathbf{q}_{\tilde{R}}$ the vectors obtained from $\mathbf{q}_L$ and $\mathbf{q}_R$ by reversing the order of the element at y by those at $l_y - y$ and using relation (40). The last equality defines the ordering denoted $\tilde{l}$ from the ordering l. One also has, according to the symmetry hypothesis,

$$\begin{aligned} \mathbf{D}_{Tl} &= \begin{bmatrix} \mathbf{D}_{T(LB)} & \mathbf{D}_{TL} & \mathbf{D}_{T(LT)} & \mathbf{D}_{T(RB)} & \mathbf{D}_{TR} & \mathbf{D}_{T(RT)} \end{bmatrix} \\ &= \begin{bmatrix} \mathbf{D}_{B(LT)} & \mathbf{D}_{B\tilde{L}} & \mathbf{D}_{B(LB)} & \mathbf{D}_{B(RT)} & \mathbf{D}_{B\tilde{R}} & \mathbf{D}_{B(RB)} \end{bmatrix} \\ &= \mathbf{D}_{B\tilde{l}} \end{aligned} \tag{47}$$

and

$$\begin{aligned} \mathbf{D}_{Bl} &= \begin{bmatrix} \mathbf{D}_{B(LB)} & \mathbf{D}_{BL} & \mathbf{D}_{B(LT)} & \mathbf{D}_{B(RB)} & \mathbf{D}_{BR} & \mathbf{D}_{B(RT)} \end{bmatrix} \\ &= \begin{bmatrix} \mathbf{D}_{T(LT)} & \mathbf{D}_{T\tilde{L}} & \mathbf{D}_{T(LB)} & \mathbf{D}_{T(RT)} & \mathbf{D}_{T\tilde{R}} & \mathbf{D}_{T(RB)} \end{bmatrix} \\ &= \mathbf{D}_{T\tilde{l}} \end{aligned} \tag{48}$$

This leads to

$$\begin{aligned} \mathbf{D}_{Tl}\lambda_y\tilde{\mathbf{q}}_l &= \mathbf{D}_{B\tilde{l}}\mathbf{q}_{\tilde{l}} &= \mathbf{D}_{Bl}\mathbf{q}_l \\ \mathbf{D}_{Bl}\lambda_y\tilde{\mathbf{q}}_l &= \mathbf{D}_{T\tilde{l}}\mathbf{q}_{\tilde{l}} &= \mathbf{D}_{Tl}\mathbf{q}_l \end{aligned} \tag{49}$$

So the symmetric solution satisfies

$$\begin{aligned} \tilde{\mathbf{f}}_B &= \mathbf{D}_{Bl}\tilde{\mathbf{q}}_l + \mathbf{D}_{BB}\tilde{\mathbf{q}}_B + \mathbf{D}_{BT}\tilde{\mathbf{q}}_T \\ &= \frac{1}{\lambda_y}\mathbf{D}_{Tl}\mathbf{q}_l + \frac{1}{\lambda_y}\mathbf{D}_{TT}\mathbf{q}_T + \frac{1}{\lambda_y}\mathbf{D}_{TB}\mathbf{q}_B \\ &= \frac{1}{\lambda_y}\mathbf{f}_T \\ &= -\mathbf{f}_B \end{aligned} \tag{50}$$

and

$$\begin{aligned} \tilde{\mathbf{f}}_T &= \mathbf{D}_{Tl}\tilde{\mathbf{q}}_l + \mathbf{D}_{TB}\tilde{\mathbf{q}}_B + \mathbf{D}_{TT}\tilde{\mathbf{q}}_T \\ &= \frac{1}{\lambda_y}\mathbf{D}_{Bl}\mathbf{q}_l + \frac{1}{\lambda_y}\mathbf{D}_{BT}\mathbf{q}_T + \frac{1}{\lambda_y}\mathbf{D}_{BB}\mathbf{q}_B \\ &= \frac{1}{\lambda_y}\mathbf{f}_B \\ &= -\frac{1}{\lambda_y}\tilde{\mathbf{f}}_B \end{aligned} \tag{51}$$

This shows that the symmetric solution is associated to the propagation constant $\frac{1}{\lambda_y}$. Using the relations (10) and (46), one can also check that

$$(\mathbf{D}_{Bl} + \lambda_y \mathbf{D}_{Tl})\tilde{\mathbf{q}}_l + (\mathbf{D}_{BB} + \mathbf{D}_{TT} + \frac{1}{\lambda_y}\mathbf{D}_{BT} + \lambda_y \mathbf{D}_{TB})\tilde{\mathbf{q}}_B = 0 \tag{52}$$

The longitudinal force vector $\tilde{\mathbf{f}}_l$ is obtained from

$$\tilde{\mathbf{f}}_l = \mathbf{D}_{ll}\tilde{\mathbf{q}}_l + \mathbf{D}_{lB}\tilde{\mathbf{q}}_B + \mathbf{D}_{lT}\tilde{\mathbf{q}}_T \tag{53}$$

and one can check that we also have

$$\tilde{\mathbf{f}}_l = \mathbf{D}_l(\frac{1}{\lambda_y})\tilde{\mathbf{q}}_l \tag{54}$$

This vector is also obtained by

$$\begin{aligned} \tilde{\mathbf{f}}_l &= \mathbf{D}_{ll}\tilde{\mathbf{q}}_l + \mathbf{D}_{lB}\tilde{\mathbf{q}}_B + \mathbf{D}_{lT}\tilde{\mathbf{q}}_T \\ &= \frac{1}{\lambda_y}\mathbf{D}_{l\tilde{l}}\mathbf{q}_l + \mathbf{D}_{\tilde{l}T}\frac{1}{\lambda_y}\mathbf{q}_T + \mathbf{D}_{\tilde{l}B}\frac{1}{\lambda_y}\mathbf{q}_B \\ &= \frac{1}{\lambda_y}\left(\mathbf{D}_{\tilde{l}l}\mathbf{q}_l + \mathbf{D}_{\tilde{l}B}\mathbf{q}_B + \mathbf{D}_{\tilde{l}T}\mathbf{q}_T\right) \end{aligned} \tag{55}$$

So that $\tilde{\mathbf{f}}_l$ is obtained from $\mathbf{f}_l$ in the same way as relation (46) meaning that

$$\tilde{\mathbf{f}}_l = \frac{1}{\lambda_y}\begin{bmatrix} \mathbf{f}_{LT} \\ \mathbf{f}_{\tilde{L}} \\ \mathbf{f}_{LB} \\ \mathbf{f}_{RT} \\ \mathbf{f}_{\tilde{R}} \\ \mathbf{f}_{RB} \end{bmatrix} \tag{56}$$

One also has the equivalent of relations (18) and (19) where $\frac{1}{\lambda_y}$ is replaced by λ_y because the symmetric solution is associated to the propagation constant $\frac{1}{\lambda_y}$.

$$\left(\lambda_x {}^t\mathbf{W}_0(\lambda_y) + {}^t\mathbf{W}_1(\lambda_y)\right)\tilde{\mathbf{f}}_l = 0 \tag{57}$$

Similarly

$$\tilde{\mathbf{q}}_l = \left(\mathbf{W}_0(\frac{1}{\lambda_y}) + \lambda_x \mathbf{W}_1(\frac{1}{\lambda_y})\right)\tilde{\mathbf{q}}_r \tag{58}$$

with

$$\tilde{\mathbf{q}}_r = \begin{bmatrix} \tilde{\mathbf{q}}_{LB} \\ \tilde{\mathbf{q}}_L \end{bmatrix} = \begin{bmatrix} \frac{1}{\lambda_y}\mathbf{q}_{LT} \\ \frac{1}{\lambda_y}\mathbf{q}_{\tilde{L}} \end{bmatrix} = \begin{bmatrix} \mathbf{q}_{LB} \\ \frac{1}{\lambda_y}\mathbf{q}_{\tilde{L}} \end{bmatrix} \tag{59}$$

Finally, using relation (54), relation (20) is transformed into

$$\left(\lambda_x {}^t\mathbf{W}_0(\lambda_y) + {}^t\mathbf{W}_1(\lambda_y)\right)\mathbf{D}_l(\frac{1}{\lambda_y})\left(\mathbf{W}_0(\frac{1}{\lambda_y}) + \lambda_x \mathbf{W}_1(\frac{1}{\lambda_y})\right)\tilde{\mathbf{q}}_r = 0 \tag{60}$$

and $\tilde{\mathbf{q}}_r$ is associated to the propagation constant λ_x in the x direction and to $\frac{1}{\lambda_y}$ in the y direction.

3.2. One-dimensional periodic functions with free boundary

We consider now functions obtained for $\lambda_{y,m} = e^{im\pi l_y/L_y}$, and their associated $\lambda_{x,n}(\lambda_{y,m})$, $\mathbf{q}_{n,m}$ solutions of the eigenproblems (21) with l_y the length of the cell along y and L_y the length of the structure along y. We define new functions by

$$\mathbf{Q}_{n,m} = \mathbf{q}_{n,m} + \tilde{\mathbf{q}}_{n,m} \tag{61}$$

and the associated forces defined on each horizontal boundary between cells.

$$\begin{aligned} \mathbf{F}^B_{n,m} &= \mathbf{f}^B_{n,m} + \tilde{\mathbf{f}}^B_{n,m} \\ \mathbf{F}^T_{n,m} &= \mathbf{f}^T_{n,m} + \tilde{\mathbf{f}}^T_{n,m} \end{aligned} \tag{62}$$

From the building of the symmetric function, one has

$$\begin{aligned} \mathbf{F}^{\overline{B}}_{n,m} &= \mathbf{f}^B_{n,m} + \tilde{\mathbf{f}}^B_{n,m} \\ &= \mathbf{f}^B_{n,m} - \mathbf{f}^B_{n,m} \\ &= 0 \\ \mathbf{F}^{\overline{T}}_{n,m} &= \mathbf{f}^{\overline{T}}_{n,m} + \tilde{\mathbf{f}}^{\overline{T}}_{n,m} \\ &= -\lambda_y^{N_y}\mathbf{f}^B_{n,m} + \frac{1}{\lambda_y^{N_y}}\mathbf{f}^B_{n,m} \\ &= 0 \end{aligned} \tag{63}$$

because λ_y is such that $\lambda_y^{2N_y} = 1$ with $L_y = N_y l_y$. The notations $\overline{B}$ and $\overline{T}$ mean the bottom and top global boundaries of the whole structure with N_y cells along y.

So these functions are eigenfunctions of the one-dimensional problem along x associated to the eigenvalues $\lambda_{x,n}$ and with free boundaries on the surfaces $y = 0$ and $y = L_y$. This means that the forces are null on the base ($\overline{B}$) and top ($\overline{T}$) global boundaries.

One can ask if two solutions associated to $\lambda_y^{(1)}$ and $1/\lambda_y^{(2)}$ can be equal. If this happens, one has

$$\mathbf{q}_T = \lambda_y^{(1)}\mathbf{q}_B \tag{64}$$

$$\mathbf{q}_T = \frac{1}{\lambda_y^{(2)}}\mathbf{q}_B \tag{65}$$

So that

$$\lambda_y^{(1)}\lambda_y^{(2)} = e^{i\pi m_1/NT_y}e^{i\pi m_2/NT_y} = 1 \tag{66}$$

with $0 \leq m_1, m_2 \leq N_y$. This can happens only if $m_1 = m_2 = 0$ or $m_1 = m_2 = N_y$ and consequently $\lambda_y^{(1)} = \lambda_y^{(2)} = 1$ or $\lambda_y^{(1)} = \lambda_y^{(2)} = -1$. In such cases the solution of the eigenproblem (21) can give a solution and its symmetric. In this case a solution is associated with its symmetric with the same λ_y to obtain a null force on the bottom and top boundaries of a substructure.

4. Global wave decomposition

4.1. General decomposition

The solution is searched under the form of waves associated to propagation constants $\lambda_{y,n} = e^{i\pi n/N_y}$ along y, for $-N_y \leq n \leq N_y - 1$, leading to the propagation constants λ^{x+} and λ^{x-} along x as defined in the end of section 2.3. One notes that $\lambda_{y,-N_y} = e^{-i\pi N_y/N_y} = e^{i\pi N_y/N_y} = \lambda_{y,N_y} = -1$, so that n ends at $N_y - 1$ otherwise the same eigenvalue would be counted twice. Along x one has propagation

constants $\lambda_{x,m} = e^{i\pi m/N_x}$, for $-N_x \leq m \leq N_x - 1$, leading to the propagation constants λ^{y+} and λ^{y-} along y. The force on the boundary X of the substructure at (p, q) can then be decomposed as

$$\begin{aligned}
\mathbf{f}_X(p,q) &= \sum_{n=-N_y}^{n=N_y-1} e^{i\pi qn/N_y} \left(\sum_{j=1}^{J_n^+} (\lambda_{nj}^{x+})^p \mathbf{f}_{Xnj}^{x+} a_{nj}^{x+} + \sum_{j=1}^{J_n^-} (\lambda_{nj}^{x-})^{p-(N_x-1)} \mathbf{f}_{Xnj}^{x-} a_{nj}^{x-} \right) \\
&+ \sum_{m=-N_x}^{m=N_x-1} e^{i\pi pm/N_x} \left(\sum_{l=1}^{L_m^+} (\lambda_{ml}^{y+})^q \mathbf{f}_{Xml}^{y+} a_{ml}^{y+} + \sum_{l=1}^{L_m^-} (\lambda_{ml}^{y-})^{q-(N_y-1)} \mathbf{f}_{Xml}^{y-} a_{ml}^{y-} \right) \\
&= \sum_{n=-N_y}^{n=N_y-1} e^{i\pi qn/N_y} \left(\mathbf{F}_{Xn}^{x+} (\mathbf{\Lambda}_n^{x+})^p \mathbf{a}_n^{x+} + \mathbf{F}_{Xn}^{x-} (\mathbf{\Lambda}_n^{x-})^{p-(N_x-1)} \mathbf{a}_n^{x-} \right) \\
&+ \sum_{m=-N_x}^{m=N_x-1} e^{i\pi pm/N_x} \left(\mathbf{F}_{Xm}^{y+} (\mathbf{\Lambda}_m^{y+})^q \mathbf{a}_m^{y+} + \mathbf{F}_{Xm}^{y-} (\mathbf{\Lambda}_m^{y-})^{q-(N_y-1)} \mathbf{a}_m^{y-} \right)
\end{aligned} \tag{67}$$

for $0 \leq p \leq N_x - 1$ and $0 \leq q \leq N_y - 1$ and where $|\lambda_{nj}^{x+}|, |\lambda_{ml}^{y+}| < 1$, $|\lambda_{nj}^{x-}|, |\lambda_{ml}^{y-}| > 1$. J_n^+, J_n^-, L_m^+, L_m^-, are the number of eigenvalues of their respective eigenproblems. Note that taking the integer $m + 2N_x$ in the last sum instead of m would lead to the same propagation constant along x. So $2N_x$ waves are sufficient for the decomposition along x and $2N_y$ along y.

One also has

$$\begin{aligned}
\mathbf{\Lambda}_n^{x+} &= diag\left(\lambda_{nj}^{x+}\right)_{j=1\ldots J_n^+}, & \mathbf{\Lambda}_n^{x-} &= diag\left(\lambda_{nj}^{x-}\right)_{j=1\ldots J_n^-} \\
\mathbf{\Lambda}_m^{y+} &= diag\left(\lambda_{ml}^{y+}\right)_{l=1\ldots L_m^+}, & \mathbf{\Lambda}_m^{y-} &= diag\left(\lambda_{ml}^{y-}\right)_{l=1\ldots L_m^-} \\
\mathbf{F}_{Xn}^{x+} &= \left[\mathbf{f}_{Xn1}^{x+}, ..., \mathbf{f}_{Xnj}^{x+}, ..., \mathbf{f}_{XnJ_n^+}^{x+}\right], & \mathbf{F}_{Xn}^{x-} &= \left[\mathbf{f}_{Xn1}^{x-}, ..., \mathbf{f}_{Xnj}^{x-} ..., \mathbf{f}_{XnJ_n^-}^{x-}\right] \\
\mathbf{F}_{Xm}^{y+} &= \left[\mathbf{f}_{Xm1}^{y+}, ..., \mathbf{f}_{Xml}^{y+} ..., \mathbf{f}_{XmL_m^+}^{y+}\right], & \mathbf{F}_{Xm}^{y-} &= \left[\mathbf{f}_{Xm1}^{y-}, ..., \mathbf{f}_{Xml}^{y-} ..., \mathbf{f}_{XmL_m^-}^{y-}\right] \\
\mathbf{a}_n^{x+} &= {}^t\left[a_{n1}^{x+}, ..., a_{nj}^{x+}, ..., a_{nJ_n^+}^{x+}\right], & \mathbf{a}_n^{x-} &= {}^t\left[a_{n1}^{x-}, ..., a_{nj}^{x-}, ..., a_{nJ_n^-}^{x-}\right] \\
\mathbf{a}_m^{y+} &= {}^t\left[a_{m1}^{y+}, ..., a_{ml}^{y+}, ..., a_{mL_m^+}^{y+}\right], & \mathbf{a}_m^{y-} &= {}^t\left[a_{m1}^{y-}, ..., a_{ml}^{y-}, ..., a_{mL_m^-}^{y-}\right]
\end{aligned} \tag{68}$$

The components of the force, for instance $\mathbf{f}_{Xnj}^{x+}$, are obtained by first solving the eigenproblem (20), leading to the eigenvectors as given in (28). Then the displacements on the longitudinal DoFs can be found from relation (16) and the displacements of the transverse DoFs by (11) and (9). Finally, the component of the force vector on all parts of the boundary of a substructure are given by relation (8).

In relation (67), we avoid taking positive powers of propagation constants of modulus greater than one by modifying the terms associated to left going waves. For these waves, the reference amplitude is taken on the right boundary (or the top boundary) of the global structure in such a way that a point inside the structure is associated with the inverse of these propagation constants which are therefore of modulus less than one and do not lead to a large modulus term.

4.2. Decomposition of force vectors on the global boundary

Now we apply this to the different parts of the global boundary. For instance, the force on the global bottom boundary can then be decomposed as (since $q = 0$, $X = B$ and at cell $(p_B, 0)$.)

$$\begin{aligned}\mathbf{f}_B(p_B) &= \sum_{n=-N_y}^{n=N_y-1} \left(\mathbf{F}_{Bn}^{x+}(\mathbf{\Lambda}_n^{x+})^{p_B}\mathbf{a}_n^{x+} + \mathbf{F}_{Bn}^{x-}(\mathbf{\Lambda}_n^{x-})^{p_B-(N_x-1)}\mathbf{a}_n^{x-}\right) \\ &+ \sum_{m=-N_x}^{m=N_x-1} e^{i\pi p_B m/N_x}\left(\mathbf{F}_{Bm}^{y+}\mathbf{a}_m^{y+} + \mathbf{F}_{Bm}^{y-}(\mathbf{\Lambda}_m^{y-})^{-(N_y-1)}\mathbf{a}_m^{y-}\right)\end{aligned} \tag{69}$$

From relations (25) and the associated discussion, one has in a general way,

$$\begin{aligned}\mathbf{\Lambda}_n^{x+} &= (\mathbf{\Lambda}_{-n}^{x-})^{-1} \\ \mathbf{\Lambda}_m^{y+} &= (\mathbf{\Lambda}_{-m}^{y-})^{-1}\end{aligned} \tag{70}$$

Supposing that the substructure is symmetric, we also have the following relation obtained from section 3.1

$$\begin{aligned}\mathbf{\Lambda}_{-n}^{x+} &= \mathbf{\Lambda}_n^{x+} \\ \mathbf{\Lambda}_{-n}^{x-} &= \mathbf{\Lambda}_n^{x-} \\ \mathbf{\Lambda}_{-n}^{y+} &= \mathbf{\Lambda}_n^{y+} \\ \mathbf{\Lambda}_{-n}^{y-} &= \mathbf{\Lambda}_n^{y-} \\ \mathbf{F}_{B(-n)}^{x+} &= -\mathbf{F}_{Bn}^{x+} \\ \mathbf{F}_{B(-n)}^{x-} &= -\mathbf{F}_{Bn}^{x-}\end{aligned} \tag{71}$$

Note that the waveforms associated with -n (or -m) are obtained without recalculation from the waveforms associated with n (or m) using the symmetries described by the relations (41), (42), (46) and (56). To build functions with global free boundaries, following the functions defined in section 3.2, one can choose the decomposition such that

$$\begin{aligned}\mathbf{a}_{-n}^{x+} &= \mathbf{a}_n^{x+} \\ \mathbf{a}_{-n}^{x-} &= \mathbf{a}_n^{x-} \\ \mathbf{a}_{-m}^{y+} &= \mathbf{a}_m^{y+} \\ \mathbf{a}_{-m}^{y-} &= \mathbf{a}_m^{y-}\end{aligned} \tag{72}$$

Inserting relations (71) and (72) into (69) leads to

$$\mathbf{f}_B(p_B) = \sum_{m=-N_x}^{m=N_x-1} e^{i\pi p_B m/N_x}\left(\mathbf{F}_{Bm}^{y+}\mathbf{a}_m^{y+} + \mathbf{F}_{Bm}^{y-}(\mathbf{\Lambda}_m^{y-})^{-(N_y-1)}\mathbf{a}_m^{y-}\right)$$

because the first sum of (69) is null. Using the relation

$$\mathbf{F}_{Tm}^{y-} + \mathbf{F}_{Bm}^{y-}\mathbf{\Lambda}_m^{y-} = 0 \tag{73}$$

we finally get

$$\mathbf{f}_B(p_B) = \sum_{m=-N_x}^{m=N_x-1} e^{i\pi p_B m/N_x}\left(\mathbf{F}_{Bm}^{y+}\mathbf{a}_m^{y+} - \mathbf{F}_{Tm}^{y-}(\mathbf{\Lambda}_m^{y-})^{-N_y}\mathbf{a}_m^{y-}\right) \tag{74}$$

In a similar way, one has

$$\begin{aligned}
\mathbf{f}_R(q_R) &= \sum_{n=-N_y}^{n=N_y-1} e^{i\pi q_R n/N_y}\left(-\mathbf{F}_{Ln}^{x+}(\mathbf{\Lambda}_n^{x+})^{N_x}\mathbf{a}_n^{x+}+\mathbf{F}_{Rn}^{x-}\mathbf{a}_n^{x-}\right)\\
\mathbf{f}_T(p_T) &= \sum_{m=-N_x}^{m=N_x-1} e^{i\pi p_T m/N_x}\left(-\mathbf{F}_{Bm}^{y+}(\mathbf{\Lambda}_m^{y+})^{N_y}\mathbf{a}_m^{y+}+\mathbf{F}_{Tm}^{y-}\mathbf{a}_m^{y-})\right)\\
\mathbf{f}_L(q_L) &= \sum_{n=-N_y}^{n=N_y-1} e^{i\pi q_L n/N_y}\left(\mathbf{F}_{Ln}^{x+}\mathbf{a}_n^{x+}-\mathbf{F}_{Rn}^{x-}(\mathbf{\Lambda}_n^{x-})^{-N_x}\mathbf{a}_n^{x-}\right)
\end{aligned} \tag{75}$$

4.3. System to solve

The preceding relations can be written in a more compact form as

$$\begin{aligned}
\mathbf{F}_{\overline{B}} &= \boldsymbol{\omega}_x\mathbf{F}_B^{y+}\mathbf{a}^{y+}-\boldsymbol{\omega}_x\mathbf{F}_T^{y-}(\mathbf{\Lambda}^{y-})^{-N_y}\mathbf{a}^{y-}\\
\mathbf{F}_{\overline{R}} &= -\boldsymbol{\omega}_y\mathbf{F}_L^{x+}(\mathbf{\Lambda}^{x+})^{N_x}\mathbf{a}^{x+}+\boldsymbol{\omega}_y\mathbf{F}_R^{x-}\mathbf{a}^{x-}\\
\mathbf{F}_{\overline{T}} &= -\boldsymbol{\omega}_x\mathbf{F}_B^{y+}(\mathbf{\Lambda}^{y+})^{N_y}\mathbf{a}^{y+}+\boldsymbol{\omega}_x\mathbf{F}_T^{y-}\mathbf{a}^{y-}\\
\mathbf{F}_{\overline{L}} &= \boldsymbol{\omega}_y\mathbf{F}_L^{x+}\mathbf{a}^{x+}-\boldsymbol{\omega}_y\mathbf{F}_R^{x-}(\mathbf{\Lambda}^{x-})^{-N_x}\mathbf{a}^{x-}
\end{aligned} \tag{76}$$

with the overline on $\overline{L}$ meaning the global left boundary and for instance

$$\begin{aligned}
\mathbf{F}_{\overline{L}} &= \begin{pmatrix}\mathbf{f}_L(0)\\ \mathbf{f}_L(1)\\ \vdots\\ \mathbf{f}_L(N_y-1)\end{pmatrix}\\
\mathbf{F}_L^{x+} &= diag\left(\mathbf{F}_{L(-N_y)}^{x+},...,\mathbf{F}_{Ln}^{x+},...,\mathbf{F}_{LN_y-1}^{x+}\right)\\
\mathbf{F}_R^{x-} &= diag\left(\mathbf{F}_{R(-N_y)}^{x-},...,\mathbf{F}_{Rn}^{x-},...,\mathbf{F}_{RN_y-1}^{x-}\right)\\
\mathbf{\Lambda}^{x-} &= diag\left(\mathbf{\Lambda}_{-N_y}^{x-},...,\mathbf{\Lambda}_n^{x-},...,\mathbf{\Lambda}_{N_y-1}^{x-}\right)\\
\boldsymbol{\omega}_y &= \left(e^{iqn\pi/N_y}\mathbf{I}_{qn}\right)_{0\le q\le N_y-1,-N_y\le n\le N_y-1}\\
&= \left(\lambda_y^{qn}\mathbf{I}_{qn}\right)_{0\le q\le N_y-1,-N_y\le n\le N_y-1}
\end{aligned} \tag{77}$$

with $\lambda_y = e^{i\pi/N_y}$, $\mathbf{I}_{qn} = \mathbf{I}_{n_r^y\times n_r^y}$ and $n_r^y = n_{LB}+n_L$ where n_{LB} is the number of DoFs in the corner LB and n_L the number of DoFs in the part L of the boundary (the left side without corners). The size of $\mathbf{F}_{Ln}^{x+}$ is $n_r^y\times J_n^+$ and that of $\mathbf{F}_{Rn}^{x-}$ is $n_r^y\times J_n^-$. The size of $\mathbf{F}_{\overline{L}}$ is $N_L = N_y n_r^y$. The sum of the sizes of the vectors of wave amplitude $\mathbf{a}^{y-}$ and $\mathbf{a}^{y+}$ is $4N_x(n_{LB}+n_B)$ because there are $2N_x$ types of waves and each one is associated with an eigenproblem of size $n_{LB}+n_B$ (with $2(n_{LB}+n_B)$ solutions). In the same way, the sum of the sizes of the vectors of wave amplitude $\mathbf{a}^{x-}$ and $\mathbf{a}^{x+}$ is $4N_y(n_{LB}+n_L)$. Thus, globally, there are $4N_x(n_{LB}+n_B)+4N_y(n_{LB}+n_L)$ amplitudes of waves which is two times the number of DoFs on the boundary of the global structure. If we use relations (72), the number of wave amplitudes becomes the number of DoFs on the global boundary.

A similar relation can be written for the right boundary. For the top boundary, one has for

instance.

$$\begin{aligned}
\mathbf{F}_{\overline{T}} &= \begin{pmatrix} \mathbf{f}_T(0) \\ \mathbf{f}_T(1) \\ \vdots \\ \mathbf{f}_T(N_x-1) \end{pmatrix} \\
\mathbf{F}_T^{y-} &= diag\left(\mathbf{F}_{T(-N_x)}^{y-},...,\mathbf{F}_{Tm}^{y-},...,\mathbf{F}_{TN_x-1}^{y-}\right) \\
\mathbf{F}_B^{y+} &= diag\left(\mathbf{F}_{B(-N_x)}^{y+},...,\mathbf{F}_{Bm}^{y+},...,\mathbf{F}_{BN_x-1}^{y+}\right) \\
\mathbf{\Lambda}^{y+} &= diag\left(\mathbf{\Lambda}_{-N_x}^{y+},...,\mathbf{\Lambda}_{m}^{y+},...,\mathbf{\Lambda}_{N_x-1}^{y+}\right) \\
\boldsymbol{\omega}_x &= \left(e^{ipm\pi/N_x}\mathbf{I}_{pnm}\right)_{0\leq p\leq N_x-1,-N_x\leq m\leq N_x-1} \\
&= \left(\lambda_x^{pm}\mathbf{I}_{pm}\right)_{0\leq p\leq N_x-1,-N_x\leq m\leq N_x-1}
\end{aligned} \tag{78}$$

with $\lambda_x = e^{i\pi/N_x}$ and $\mathbf{I}_{pm} = \mathbf{I}_{n_r^x\times n_r^x}$ and $n_r^x = n_{LB}+n_B$. The size of $\mathbf{F}_{Bm}^{y+}$ is $n_r^x \times L_n^+$ and that of $\mathbf{F}_{Tm}^{y-}$ is $n_r^x \times L_n^-$. In matrix form this yields the following system

$$\begin{pmatrix} \mathbf{F}_{\overline{B}} \\ \mathbf{F}_{\overline{R}} \\ \mathbf{F}_{\overline{T}} \\ \mathbf{F}_{\overline{L}} \end{pmatrix} = \begin{pmatrix} \mathbf{o}_{N_B\times J^+} & \mathbf{o}_{N_B\times J^-} & \boldsymbol{\omega}_x\mathbf{F}_B^{y+} & -\boldsymbol{\omega}_x\mathbf{F}_T^{y-}(\mathbf{\Lambda}^{y-})^{-N_y} \\ -\boldsymbol{\omega}_y\mathbf{F}_L^{x+}(\mathbf{\Lambda}^{x+})^{N_x} & \boldsymbol{\omega}_y\mathbf{F}_R^{x-} & \mathbf{o}_{N_L\times L^+} & \mathbf{o}_{N_L\times L^-} \\ \mathbf{o}_{N_B\times J^+} & \mathbf{o}_{N_B\times J^-} & -\boldsymbol{\omega}_x\mathbf{F}_B^{y+}(\mathbf{\Lambda}^{y+})^{N_y} & \boldsymbol{\omega}_x\mathbf{F}_T^{y-} \\ \boldsymbol{\omega}_y\mathbf{F}_L^{x+} & -\boldsymbol{\omega}_y\mathbf{F}_R^{x-}(\mathbf{\Lambda}^{x-})^{-N_x} & \mathbf{o}_{N_L\times L^+} & \mathbf{o}_{N_L\times L^-} \end{pmatrix} \begin{pmatrix} \mathbf{a}^{x+} \\ \mathbf{a}^{x-} \\ \mathbf{a}^{y+} \\ \mathbf{a}^{y-} \end{pmatrix} \tag{79}$$

with for instance the size of $\mathbf{F}_{\overline{B}}$ is $N_B = N_x(n_{LB}+n_B)$ the number of DoFs on the global bottom boundary minus the bottom right corner and $J^+ = \sum_{n=-N_x}^{n=N_x-1} J_n^+$, the number of positive waves along x.

5. Fast solution for the two-dimensional periodic structures

5.1. Symmetric relations

It is possible to solve the system (79) directly, but we prefer to solve another system to take advantage of a Fourier transform and solve it by FFT. Consider relation (74), one has

$$\begin{aligned}
\mathbf{f}_B(p_B) &= \sum_{m=-N_x}^{m=N_x-1} e^{i\pi p_B m/N_x}\left(\mathbf{F}_{Bm}^{y+}\mathbf{a}_m^{y+} - \mathbf{F}_{Tm}^{y-}(\mathbf{\Lambda}_m^{y-})^{-N_y}\mathbf{a}_m^{y-}\right) \\
&= \sum_{m=-N_x+1}^{m=N_x} e^{-i\pi p_B m/N_x}\left(\mathbf{F}_{B(-m)}^{y+}\mathbf{a}_m^{y+} - \mathbf{F}_{T(-m)}^{y-}(\mathbf{\Lambda}_m^{y-})^{-N_y}\mathbf{a}_m^{y-}\right)
\end{aligned} \tag{80}$$

Note that $\lambda_{x,-N_x} = \lambda_{x,N_x} = -1$, and for instance $\mathbf{F}_{B(-N_x)}^{y+} = \mathbf{F}_{BN_x}^{y+}$. So that one also has

$$\mathbf{f}_B(p_B) = \sum_{m=-N_x}^{m=N_x-1} e^{-i\pi p_B m/N_x}\left(\mathbf{F}_{B(-m)}^{y+}\mathbf{a}_m^{y+} - \mathbf{F}_{T(-m)}^{y-}(\mathbf{\Lambda}_m^{y-})^{-N_y}\mathbf{a}_m^{y-}\right) \tag{81}$$

Note also that from the equivalent of relation (56) applied to the bottom boundary, for instance, $\mathbf{F}_{B(-m)}^{y+} = \frac{1}{\lambda_{x,m}}\tilde{\mathbf{F}}_{B(m)}^{y+}$, and a similar relation for the top component, so that we finally get

$$\mathbf{f}_B(p_B) = \sum_{m=-N_x}^{m=N_x-1} e^{-i\pi(p_B+1)m/N_x}\left(\tilde{\mathbf{F}}_{Bm}^{y+}\mathbf{a}_m^{y+} - \tilde{\mathbf{F}}_{Tm}^{y-}(\mathbf{\Lambda}_m^{y-})^{-N_y}\mathbf{a}_m^{y-}\right)$$

and

$$\tilde{\mathbf{f}}_B(p_B) = \sum_{m=-N_x}^{m=N_x-1} e^{-i\pi(p_B+1)m/N_x} \left(\mathbf{F}_{Bm}^{y+} \mathbf{a}_m^{y+} - \mathbf{F}_{Tm}^{y-} (\mathbf{\Lambda}_m^{y-})^{-N_y} \mathbf{a}_m^{y-} \right)$$

with $\tilde{\mathbf{f}}_B(p_B)$ obtained from $\mathbf{f}_B(p_B)$ by inverting the DoFs on the bottom boundary on each cell between 0 and l_x. The function $\mathbf{f}_B(p_B)$ can now be defined for $-N_x \leq p_B \leq N_x - 1$ with $\mathbf{f}_B(-p_B-1) = \tilde{\mathbf{f}}_B(p_B)$.

The global system to solve is then

$$\begin{pmatrix} \mathbf{F}_{\overline{B}} \\ \tilde{\mathbf{F}}_{\overline{B}} \\ \mathbf{F}_{\overline{R}} \\ \tilde{\mathbf{F}}_{\overline{R}} \\ \mathbf{F}_{\overline{T}} \\ \tilde{\mathbf{F}}_{\overline{T}} \\ \mathbf{F}_{\overline{L}} \\ \tilde{\mathbf{F}}_{\overline{L}} \end{pmatrix} = \begin{pmatrix} \mathbf{o}_{N_B \times J^+} & \mathbf{o}_{N_B \times J^-} & \boldsymbol{\omega}_x^+ \mathbf{F}_B^{y+} & -\boldsymbol{\omega}_x^+ \mathbf{F}_T^{y-} (\mathbf{\Lambda}^{y-})^{-N_y} \\ \mathbf{o}_{N_B \times J^+} & \mathbf{o}_{N_B \times J^-} & \boldsymbol{\omega}_x^- \mathbf{F}_B^{y+} & -\boldsymbol{\omega}_x^- \mathbf{F}_T^{y-} (\mathbf{\Lambda}^{y-})^{-N_y} \\ -\boldsymbol{\omega}_y^+ \mathbf{F}_L^{x+} (\mathbf{\Lambda}^{x+})^{N_x} & \boldsymbol{\omega}_y^+ \mathbf{F}_R^{x-} & \mathbf{o}_{N_L \times L^+} & \mathbf{o}_{N_L \times L^-} \\ -\boldsymbol{\omega}_y^- \mathbf{F}_L^{x+} (\mathbf{\Lambda}^{x+})^{N_x} & \boldsymbol{\omega}_y^- \mathbf{F}_R^{x-} & \mathbf{o}_{N_L \times L^+} & \mathbf{o}_{N_L \times L^-} \\ \mathbf{o}_{N_B \times J^+} & \mathbf{o}_{N_B \times J^-} & -\boldsymbol{\omega}_x^+ \mathbf{F}_B^{y+} (\mathbf{\Lambda}^{y+})^{N_y} & \boldsymbol{\omega}_x^+ \mathbf{F}_T^{y-} \\ \mathbf{o}_{N_B \times J^+} & \mathbf{o}_{N_B \times J^-} & -\boldsymbol{\omega}_x^- \mathbf{F}_B^{y+} (\mathbf{\Lambda}^{y+})^{N_y} & \boldsymbol{\omega}_x^- \mathbf{F}_T^{y-} \\ \boldsymbol{\omega}_y^+ \mathbf{F}_L^{x+} & -\boldsymbol{\omega}_y^+ \mathbf{F}_R^{x-} (\mathbf{\Lambda}^{x-})^{-N_x} & \mathbf{o}_{N_L \times L^+} & \mathbf{o}_{N_L \times L^-} \\ \boldsymbol{\omega}_y^- \mathbf{F}_L^{x+} & -\boldsymbol{\omega}_y^- \mathbf{F}_R^{x-} (\mathbf{\Lambda}^{x-})^{-N_x} & \mathbf{o}_{N_L \times L^+} & \mathbf{o}_{N_L \times L^-} \end{pmatrix} \begin{pmatrix} \mathbf{a}^{x+} \\ \mathbf{a}^{x-} \\ \mathbf{a}^{y+} \\ \mathbf{a}^{y-} \end{pmatrix} \tag{82}$$

with

$$\tilde{\mathbf{F}}_{\overline{B}} = \begin{pmatrix} \tilde{\mathbf{f}}_B(N_x - 1) \\ \vdots \\ \tilde{\mathbf{f}}_B(0) \end{pmatrix}, \qquad \mathbf{F}_{\overline{B}} = \begin{pmatrix} \mathbf{f}_B(0) \\ \vdots \\ \mathbf{f}_B(N_x - 1) \end{pmatrix}$$

$$\boldsymbol{\omega}_x^- = \begin{pmatrix} e^{-i\pi N_x m/N_x} \mathbf{I}_{n_r^x \times n_r^x} \\ e^{-i\pi(N_x-1)m/N_x} \mathbf{I}_{n_r^x \times n_r^x} \\ \vdots \\ e^{-i2\pi m/N_x} \mathbf{I}_{n_r^x \times n_r^x} \\ e^{-i\pi m/N_x} \mathbf{I}_{n_r^x \times n_r^x} \end{pmatrix}_{-N_x \leq m \leq N_x - 1}, \qquad \boldsymbol{\omega}_x^+ = \begin{pmatrix} \mathbf{I}_{n_r^x \times n_r^x} \\ e^{i\pi m/N_x} \mathbf{I}_{n_r^x \times n_r^x} \\ \vdots \\ e^{i\pi(N_x-2)m/N_x} \mathbf{I}_{n_r^x \times n_r^x} \\ e^{i\pi(N_x-1)m/N_x} \mathbf{I}_{n_r^x \times n_r^x} \end{pmatrix}_{-N_x \leq m \leq N_x - 1} \tag{83}$$

The global system (82) is a square system with a size which equals two times the number of DoFs on the boundary of the global structure. It can be decomposed into two subsytems because the left/right and bottom/top boundaries are decoupled. This leads to

$$\begin{aligned} \begin{pmatrix} \mathbf{F}_{\overline{R}} \\ \tilde{\mathbf{F}}_{\overline{R}} \\ \mathbf{F}_{\overline{L}} \\ \tilde{\mathbf{F}}_{\overline{L}} \end{pmatrix} &= \begin{pmatrix} -\boldsymbol{\omega}_y^+ \mathbf{F}_L^{x+} (\mathbf{\Lambda}^{x+})^{N_x} & \boldsymbol{\omega}_y^+ \mathbf{F}_R^{x-} \\ -\boldsymbol{\omega}_y^- \mathbf{F}_L^{x+} (\mathbf{\Lambda}^{x+})^{N_x} & \boldsymbol{\omega}_y^- \mathbf{F}_R^{x-} \\ \boldsymbol{\omega}_y^+ \mathbf{F}_L^{x+} & -\boldsymbol{\omega}_y^+ \mathbf{F}_R^{x-} (\mathbf{\Lambda}^{x-})^{-N_x} \\ \boldsymbol{\omega}_y^- \mathbf{F}_L^{x+} & -\boldsymbol{\omega}_y^- \mathbf{F}_R^{x-} (\mathbf{\Lambda}^{x-})^{-N_x} \end{pmatrix} \begin{pmatrix} \mathbf{a}^{x+} \\ \mathbf{a}^{x-} \end{pmatrix} \\ &= \begin{pmatrix} \boldsymbol{\omega}_y^+ & \mathbf{o}_{N_L \times N_L} \\ \boldsymbol{\omega}_y^- & \mathbf{o}_{N_L \times N_L} \\ \mathbf{o}_{N_L \times N_L} & \boldsymbol{\omega}_y^+ \\ \mathbf{o}_{N_L \times N_L} & \boldsymbol{\omega}_y^- \end{pmatrix} \begin{pmatrix} -\mathbf{F}_L^{x+} (\mathbf{\Lambda}^{x+})^{N_x} & \mathbf{F}_R^{x-} \\ \mathbf{F}_L^{x+} & -\mathbf{F}_R^{x-} (\mathbf{\Lambda}^{x-})^{-N_x} \end{pmatrix} \begin{pmatrix} \mathbf{a}^{x+} \\ \mathbf{a}^{x-} \end{pmatrix} \end{aligned} \tag{84}$$

and

$$\begin{pmatrix} \mathbf{F}_{\overline{B}} \\ \tilde{\mathbf{F}}_{\overline{B}} \\ \mathbf{F}_{\overline{T}} \\ \tilde{\mathbf{F}}_{\overline{T}} \end{pmatrix} = \begin{pmatrix} \boldsymbol{\omega}_x^+ \mathbf{F}_B^{y+} & -\boldsymbol{\omega}_x^+ \mathbf{F}_T^{y-} (\boldsymbol{\Lambda}^{y-})^{-N_y} \\ \boldsymbol{\omega}_x^- \mathbf{F}_B^{y+} & -\boldsymbol{\omega}_x^- \mathbf{F}_T^{y-} (\boldsymbol{\Lambda}^{y-})^{-N_y} \\ -\boldsymbol{\omega}_x^+ \mathbf{F}_B^{y+} (\boldsymbol{\Lambda}^{y+})^{N_y} & \boldsymbol{\omega}_x^+ \mathbf{F}_T^{y-} \\ -\boldsymbol{\omega}_x^- \mathbf{F}_B^{y+} (\boldsymbol{\Lambda}^{y+})^{N_y} & \boldsymbol{\omega}_x^- \mathbf{F}_T^{y-} \end{pmatrix} \begin{pmatrix} \mathbf{a}^{y+} \\ \mathbf{a}^{y-} \end{pmatrix}$$

$$= \begin{pmatrix} \boldsymbol{\omega}_x^+ & \mathbf{o}_{N_B \times N_B} \\ \boldsymbol{\omega}_x^- & \mathbf{o}_{N_B \times N_B} \\ \mathbf{o}_{N_B \times N_B} & \boldsymbol{\omega}_x^+ \\ \mathbf{o}_{N_B \times N_B} & \boldsymbol{\omega}_x^- \end{pmatrix} \begin{pmatrix} \mathbf{F}_B^{y+} & -\mathbf{F}_T^{y-} (\boldsymbol{\Lambda}^{y-})^{-N_y} \\ -\mathbf{F}_B^{y+} (\boldsymbol{\Lambda}^{y+})^{N_y} & \mathbf{F}_T^{y-} \end{pmatrix} \begin{pmatrix} \mathbf{a}^{y+} \\ \mathbf{a}^{y-} \end{pmatrix} \tag{85}$$

5.2. Use of FFT for an efficient solution

The full matrix of the FFT is given by

$$\boldsymbol{\Omega}(\lambda) = \begin{pmatrix} \mathbf{I}_{n\times n} & \mathbf{I}_{n\times n} & \mathbf{I}_{n\times n} & \mathbf{I}_{n\times n} & \dots & \mathbf{I}_{n\times n} \\ \mathbf{I}_{n\times n} & \lambda\mathbf{I}_{n\times n} & \lambda^2\mathbf{I}_{n\times n} & \lambda^3\mathbf{I}_{n\times n} & \dots & \lambda^{2N-1}\mathbf{I}_{n\times n} \\ \mathbf{I}_{n\times n} & \lambda^2\mathbf{I}_{n\times n} & \lambda^4\mathbf{I}_{n\times n} & \lambda^6\mathbf{I}_{n\times n} & \dots & \lambda^{2(2N-1)}\mathbf{I}_{n\times n} \\ \mathbf{I}_{n\times n} & \lambda^3\mathbf{I}_{n\times n} & \lambda^6\mathbf{I}_{n\times n} & \lambda^9\mathbf{I}_{n\times n} & \dots & \lambda^{3(2N-1)}\mathbf{I}_{n\times n} \\ \vdots & \vdots & \vdots & \vdots & \ddots & \vdots \\ \mathbf{I}_{n\times n} & \lambda^{2N-1}\mathbf{I}_{n\times n} & \lambda^{2(2N-1)}\mathbf{I}_{n\times n} & \lambda^{3(2N-1)}\mathbf{I}_{n\times n} & \dots & \lambda^{(2N-1)(2N-1)}\mathbf{I}_{n\times n} \end{pmatrix}$$

with $\lambda = e^{-i\pi/N}$. Note that the sign in the exponential is opposite to the sign used to define $\lambda_{y,n}$ and $\lambda_{x,m}$. So one has the relation

$$\boldsymbol{\Omega}(\lambda_y) \begin{pmatrix} \boldsymbol{\omega}_y^+ \\ \boldsymbol{\omega}_y^- \end{pmatrix} = 2N_y \mathbf{I}_{2N_L \times 2N_L} \tag{86}$$

because this is the FFT matrix and its inverse up to the factor $2N_y$. In this case $\lambda_y = e^{-i\pi/N_y}$ and $n_r^y = n_{LB} + n_L$. Now from (84), one has

$$\begin{pmatrix} fft \begin{pmatrix} \mathbf{F}_{\overline{R}} \\ \tilde{\mathbf{F}}_{\overline{R}} \end{pmatrix} \\ fft \begin{pmatrix} \mathbf{F}_{\overline{L}} \\ \tilde{\mathbf{F}}_{\overline{L}} \end{pmatrix} \end{pmatrix} = \begin{pmatrix} \boldsymbol{\Omega}(\lambda_y) & \mathbf{o}_{2N_L \times 2N_L} \\ \mathbf{o}_{2N_L \times 2N_L} & \boldsymbol{\Omega}(\lambda_y) \end{pmatrix} \begin{pmatrix} \mathbf{F}_{\overline{R}} \\ \tilde{\mathbf{F}}_{\overline{R}} \\ \mathbf{F}_{\overline{L}} \\ \tilde{\mathbf{F}}_{\overline{L}} \end{pmatrix}$$

$$= \begin{pmatrix} \boldsymbol{\Omega}(\lambda_y) & \mathbf{o}_{2N_L \times 2N_L} \\ \mathbf{o}_{2N_L \times 2N_L} & \boldsymbol{\Omega}(\lambda_y) \end{pmatrix} \begin{pmatrix} \boldsymbol{\omega}_y^+ & \mathbf{o}_{N_L \times N_L} \\ \boldsymbol{\omega}_y^- & \mathbf{o}_{N_L \times N_L} \\ \mathbf{o}_{N_L \times N_L} & \boldsymbol{\omega}_y^+ \\ \mathbf{o}_{N_L \times N_L} & \boldsymbol{\omega}_y^- \end{pmatrix}$$

$$\times \begin{pmatrix} -\mathbf{F}_L^{x+} (\boldsymbol{\Lambda}^{x+})^{N_x} & \mathbf{F}_R^{x-} \\ \mathbf{F}_L^{x+} & -\mathbf{F}_R^{x-} (\boldsymbol{\Lambda}^{x-})^{-N_x} \end{pmatrix} \begin{pmatrix} \mathbf{a}^{x+} \\ \mathbf{a}^{x-} \end{pmatrix}$$

$$= 2N_y \begin{pmatrix} -\mathbf{F}_L^{x+} (\boldsymbol{\Lambda}^{x+})^{N_x} & \mathbf{F}_R^{x-} \\ \mathbf{F}_L^{x+} & -\mathbf{F}_R^{x-} (\boldsymbol{\Lambda}^{x-})^{-N_x} \end{pmatrix} \begin{pmatrix} \mathbf{a}^{x+} \\ \mathbf{a}^{x-} \end{pmatrix} \tag{87}$$

As the right hand side matrix is made of block diagonal matrices, this relation can be decoupled along each component of the Fourier transform. For example, we get

$$\begin{pmatrix} \mathcal{F}_{Rn} \\ \mathcal{F}_{Ln} \end{pmatrix} = 2N_y \begin{pmatrix} -\mathbf{F}_{Ln}^{x+} (\boldsymbol{\Lambda}_n^{x+})^{N_x} & \mathbf{F}_{Rn}^{x-} \\ \mathbf{F}_{Ln}^{x+} & -\mathbf{F}_{Rn}^{x-} (\boldsymbol{\Lambda}_n^{x-})^{-N_x} \end{pmatrix} \begin{pmatrix} \mathbf{a}_n^{x+} \\ \mathbf{a}_n^{x-} \end{pmatrix} \tag{88}$$

with for instance $\mathcal{F}_{Rn}$ the n^{th} component of $fft \begin{pmatrix} \mathbf{F}_{\overline{R}} \\ \tilde{\mathbf{F}}_{\overline{R}} \end{pmatrix}$.

The solution of this small size system gives the n^{th} component of the amplitude. The same thing can be done for the bottom/top components. The solution in any substructure can be found from of relation (67) for each boundary of a substructure. Then, relation (6) yields the displacement at the boundary of the substructure and (3) the displacements at the interior DoFs.

6. Numerical examples

6.1. Validation with a homogeneous structure

We first consider the case of the Helmholtz equation (modelling acoustic propagation or a membrane vibration) on a homogeneous medium divided into rectangular substructures. This will be described in the following as example one. The equation is

$$\begin{aligned} \Delta p + k^2 p &= 0 \ \ in \ \ \Omega, \\ \frac{\partial p}{\partial n} &= q_0 \ \ over \ \partial\Omega \end{aligned} \tag{89}$$

with $k = \omega/c$, ω the circular frequency and $c = 343m/s$ the sound velocity in case of acoustic propagation. The structure Ω is divided into $N_x \times N_y$ substructures of size $L_x \times L_y$. q_0 is a given function on the boundary. In this case, it is simple to find an analytical solution to estimate the accuracy of the proposed method. For example, an analytical solution is provided by $p_0(\mathbf{x}) = \frac{i}{4}H_0(k|\mathbf{x} - \mathbf{x}_s|)$ for a point source $\mathbf{x}_s$ outside the domain Ω. If we use as boundary condition its normal derivative on the global structure given by $q_0 = \frac{\partial}{\partial n}p_0$, the solution of the numerical problem inside the structure should be p_0. We compare the results of the analytical solution, a full Finite Element (FEM) solution, a one-dimensional WFE and the present two-dimensional WFE method in table 1 for structures with 5×5 and 25×25 substructures. The one-dimensional WFE is the classical approach as described for instance in [1–14]. The substructures are meshed with 10×10 quadratic 8 nodes elements, leading to 20 nodes per wavelength at 4000 Hz which is quite sufficient to get a good accuracy for each numerical solution. The mesh for the case of structures made of 5×5 substructures is shown in figure 4 with the borders of the substructures marked in red. The dimensions of a substructure are $L_x = L_y = 0.1m$ and the position of the source used to build the analytical solution is at $\mathbf{x}_s = (-0.5m, -0.5m)$. The computations are done at the three points $(0, 0)$, (L_x, L_y) and $(5L_x, 5L_y)$, the point $(0, 0)$ being the left bottom corner of the whole structure. It can be observed in table 1 that there is a perfect agreement between all the numerical methods and consequently the accuracy of the 2D WFE is the same as that of the full FEM, neither better nor worse.

6.2. Substructures with one hole

We consider now the second example of a substructure with a circular central hole of radius $0.02m$ as in figure 5. All the other properties are the same as before. The mesh is made of 654 nodes with linear triangular elements obtained from gmsh. The boundary condition is obtained as in the precedent example. The structure is made of 25×25 substructures and computed at 1000Hz. The real parts are shown in figure 6 for the full FEM computation and for the 2D WFE. The modulus of the difference between the two solutions is also plotted. It can be seen that the value of the difference is less than 0.03% that of the solution. A perfect agreement between the two computations is thus observed. The same computation is also made for structures of increasing sizes between $N \times N = 10 \times 10$ substructures and $N \times N = 1000 \times 1000$. The computing time is shown in figure 7 for the 2D WFE. For the FEM, the computation is only done up to 200×200 substructures. The computing time is strongly increasing for the FEM while it increases only mildly for the 2D WFE. For the WFE, different computing times are presented. First, the computing time for getting the amplitudes of the wave and getting the solution at one point in the domain, then the computing time for getting the solution at all nodes on a substructure and finally the computing time for getting the solution at all nodes of the global

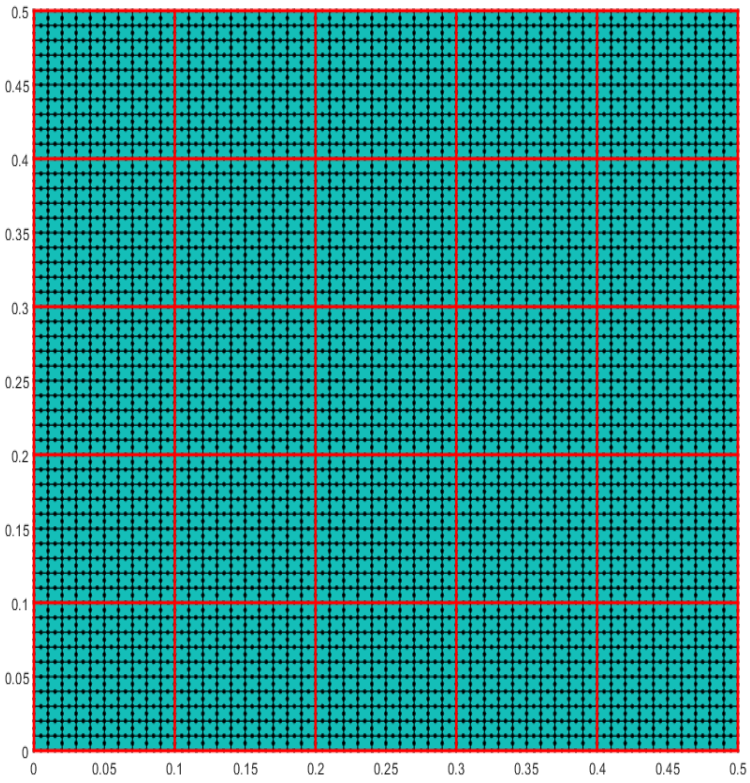

Figure 4: Mesh of a structure made of 5x5 substructures (sizes in m).

	$N_x \times N_y = 5 \times 5$			
100Hz	Analytic	WFE 1D	WFE 2D	FEM
$(0,0)$	$-0.071+0.156i$	$-0.071+0.156i$	$-0.071+0.156i$	$-0.071+0.156i$
(L_x,L_y)	$-0.101+0.120i$	$-0.101+0.120i$	$-0.101+0.120i$	$-0.101+0.120i$
$(5L_x,5L_y)$	$-0.121-0.023i$	$-0.121-0.023i$	$-0.121-0.023i$	$-0.121-0.023i$
4000Hz	Analytic	WFE 1D	WFE 2D	FEM
$(0,0)$	$-0.019+0.020i$	$-0.022+0.012i$	$-0.022+0.012i$	$-0.022+0.012i$
(L_x,L_y)	$0.025+0.003i$	$0.028+0.010i$	$0.028+0.010i$	$0.028+0.010i$
$(5L_x,5L_y)$	$-0.015-0.013i$	$-0.018-0.021i$	$-0.018-0.021i$	$-0.018-0.021i$
	$N_x \times N_y = 25 \times 25$			
100Hz	Analytic	WFE 1D	WFE 2D	FEM
$(0,0)$	$-0.071+0.156i$	$-0.071+0.156i$	$-0.071+0.156i$	$-0.071+0.156i$
(L_x,L_y)	$-0.101+0.120i$	$-0.101+0.120i$	$-0.101+0.120i$	$-0.101+0.120i$
$(5L_x,5L_y)$	$-0.121-0.023i$	$-0.121-0.023i$	$-0.121-0.023i$	$-0.121-0.023i$
4000Hz	Analytic	WFE 1D	WFE 2D	FEM
$(0,0)$	$-0.019+0.020i$	$-0.024+0.021i$	$-0.024+0.021i$	$-0.024+0.021i$
(L_x,L_y)	$0.025+0.003i$	$0.028+0.003i$	$0.028+0.003i$	$0.028+0.003i$
$(5L_x,5L_y)$	$-0.015-0.013i$	$-0.017-0.018i$	$-0.017-0.018i$	$-0.017-0.018i$

Table 1: Comparison of the solution for different methods, number of substructures, frequencies and computation points for example one.

structure. We see that the calculation time is mainly conditioned by postprocessing and the number of nodes where we wish to obtain the solution. The computing time to get the solution at one point is a few seconds by the present 2D WFE and a few minutes to get the solution on the whole structure. In term of memory, the finite element calculation with 200 substructures requires a dynamic stiffness matrix with 169×10^6 non-zero coefficients while the proposed method, which does not include a large matrix since the calculation is done independently for each order of the Fourier coefficients, does not therefore need a lot of memory. Note that for the 1000×1000 structure, the number of nodes for a classical FEM computation would be about 650 millions. This problem is solved with Matlab on a personal computer with a memory of 64GB and a processor Intel Core(TM) i9-12900.

6.3. Substructures with five holes

We consider now a more complex geometry with five holes as shown in figure 8. This is the third example. The mesh of a substructure contains 2552 nodes and is made with linear triangular elements. The total structure contains 20×20 substructures. The excitation is created by a unit point source at point $\mathbf{x}_s = (-0.5m, -0.5m)$ to create a load on the global boundary as the normal derivative of the function $p_0(\mathbf{x}) = \frac{i}{4} H_0(k|\mathbf{x} - \mathbf{x}_s|)$. Note that in the computation, the loading is indeed applied on the boundary of the domain only in order to correspond to the field of the source in $\mathbf{x}_s$. As this source is external to the domain studied, there is no loading internal to the domain. The size of a substructure is $L_x = L_y = 1m$ and the central hole has a radius $0.15m$ while the other holes have a radius of $0.05m$. The centres of the small holes are located at $0.15m$ from the boundary. As the boundary condition is applied only on the external boundary of the whole structure but not at the boundary of the internal holes, there is no analytical solution in this case. We compare the FEM and WFE 2D solutions at the corners $(0,0)$ and $(20L_x, 20L_y)$ in figure 9. There is a perfect agreement between the FEM and WFE solutions for the two points. Some resonances can be seen in the figure. Figure 9(c) plot the modulus of the difference between the FEM and WFE solutions. Globally the difference is quite small. One can only see an increase in the difference near the resonance frequencies.

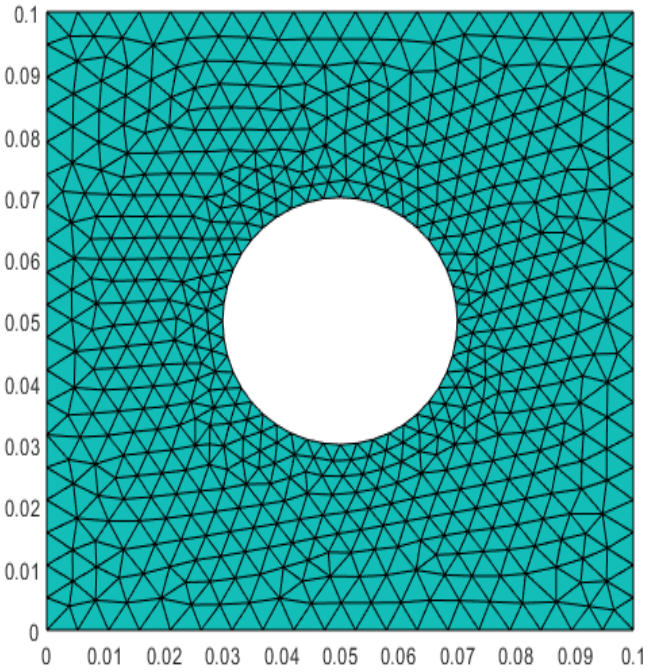

Figure 5: Substructure with a central hole (sizes in m).

6.4. Structures with resonators

We consider now the fourth case with the same geometry as in the precedent example but the holes are now filled, see figure 10. The small holes are filled with a material that has two times the matrix sound velocity while the central hole has a material with five time the matrix sound velocity. The excitation is created by a plane wave at the left boundary only while the other parts of the boundary are free. So one has $q_0(0, y) = -ik$ on the left boundary and 0 for the other parts of the boundary.

Figure 11 presents the maximum value of the modulus of the propagation constant $|\lambda_x|$ for $\lambda_y = 1$. One can clearly see a stop band around the frequency 180Hz and a smaller one near 350Hz for functions associated to $\lambda_y = 1$ and so periodic along y with a period l_y. To have another view of this effect, we define a transmission factor as the solution on the right boundary over the solution on the left boundary defined by

$$T = \frac{\left(\sum_{i \text{ on right boundary}} |u_i|^2\right)^{1/2}}{\left(\sum_{i \text{ on left boundary}} |u_i|^2\right)^{1/2}} \tag{90}$$

where u_i is the solution at node i. Figure 12 presents this transmission factor for a structure made of 40×40 substructures and clearly shows the stop band effect near 180Hz and 350Hz. Note that this curve is obtained with 400 frequency points and with a calculation time of 654 seconds, or 1.6s per point.

Figures 13 present the FEM and WFE 2D solutions for the frequency 180Hz. The effect of the band gap is clearly seen by the progressive attenuation of the solution as we move along x. The plot of the modulus of the difference between the FEM and WFE solutions show the very good agreement between the two solutions. A plot of the detailed solution for the substructure at $(19, 9)$ is also seen (The numbering of substructures starts at zero). For this low frequency the solution is rather uniform

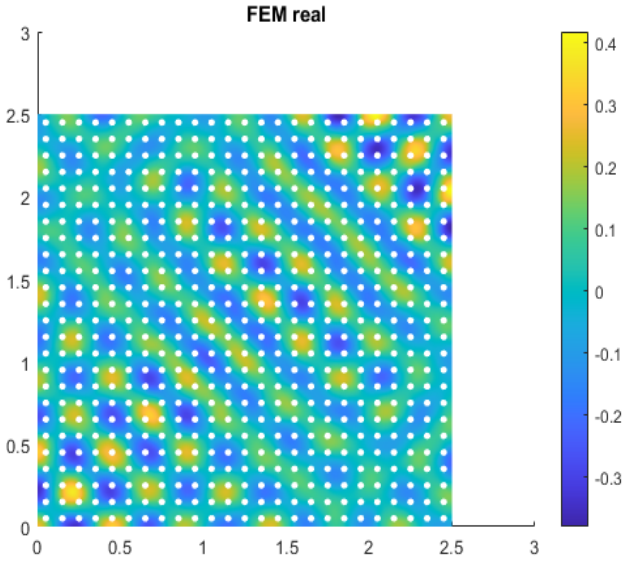

(a) FEM solution at 1000z, real part.

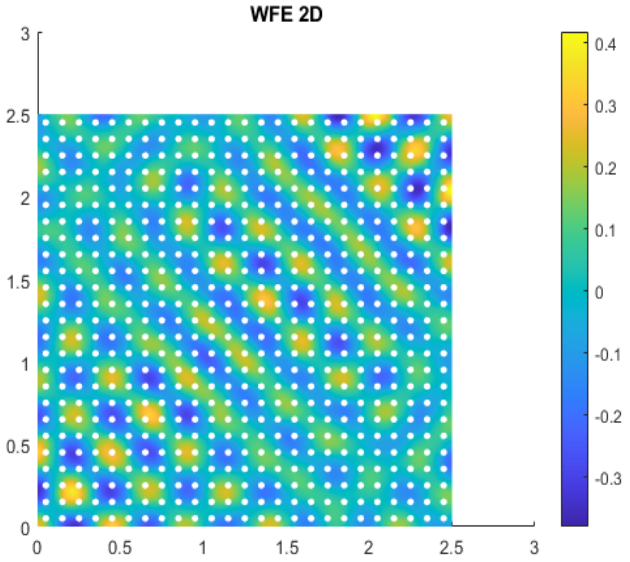

(b) WFE 2D at 1000Hz, real part.

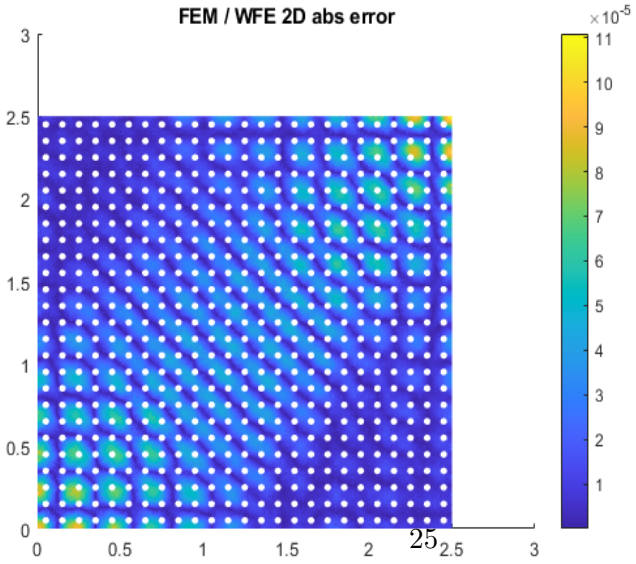

(c) Difference FEM/WFE, modulus.

Figure 6: Comparison of FEM and WFE 2D solutions for a 25×25 structure made of substructures with holes, example two.

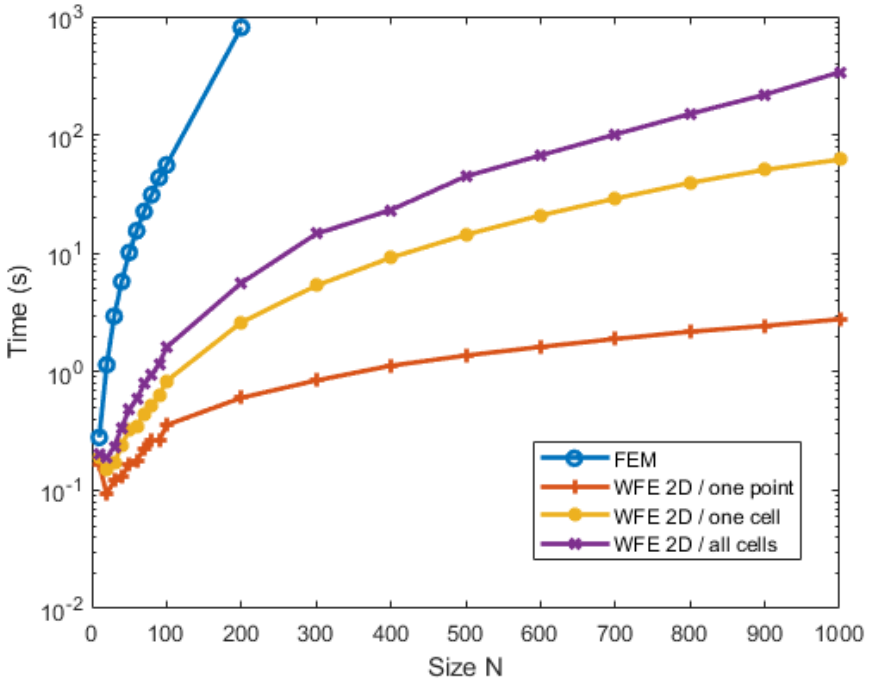

Figure 7: Computing times of the second example for the classical FEM computation and for the WFE in case of the solution at one node, at all nodes on a substructure or at all nodes on the global structure.

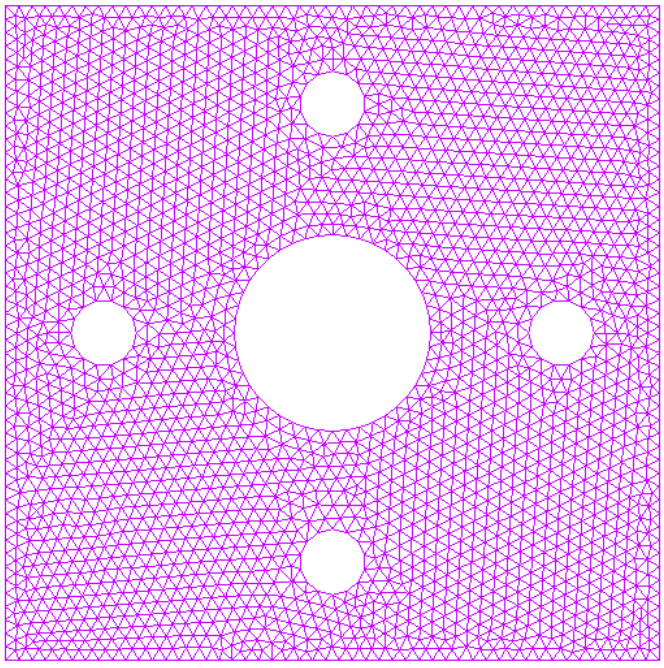

Figure 8: Substructure with five holes.

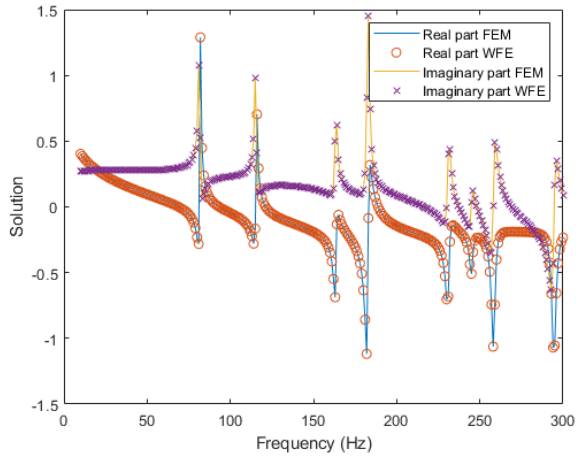

(a)

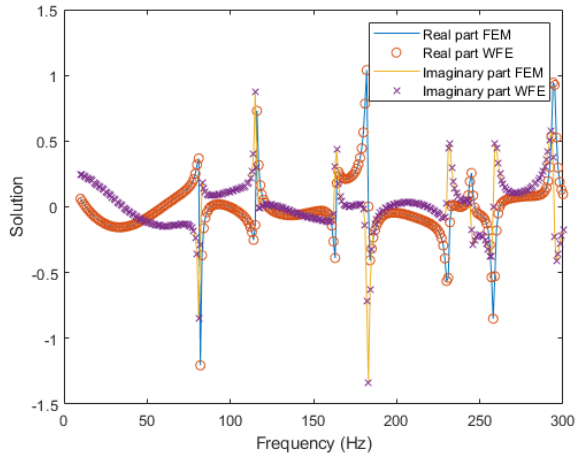

(b)

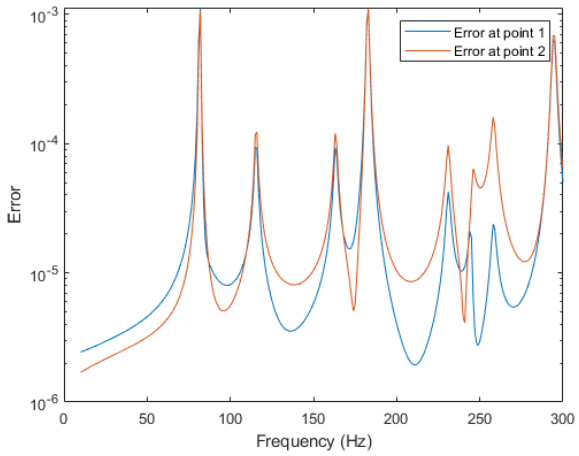

(c)

Figure 9: Comparison of the FEM and WFE 2D solutions at two corners of the global structure: (a) Comparison of the real and imaginary parts of the FEM and WFE 2D solutions at point $(0, 0)$ for the third example, (b) Comparison of the real and imaginary parts of the FEM and WFE 2D solutions at point $(20L_x, 20L_y)$ for the third example and (c) Modulus of the difference between the FEM and WFE 2D solutions for the two points.

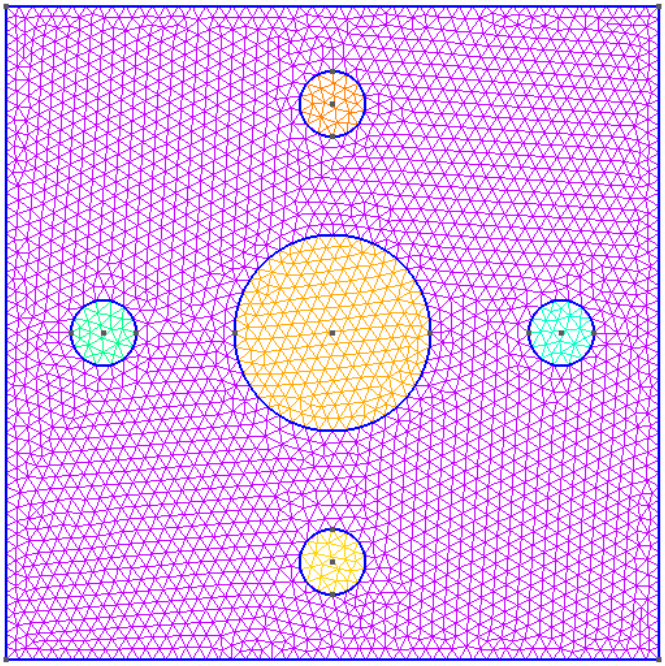

Figure 10: Mesh of a substructure with resonators.

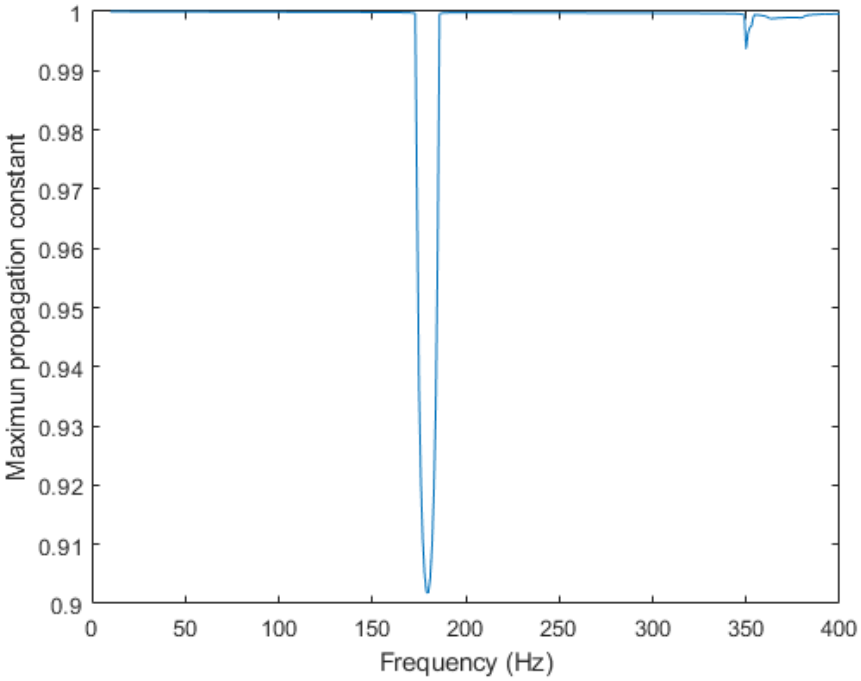

Figure 11: Maximum modulus of the propagation constant $|\lambda_x|$ for $\lambda_y = 1$.

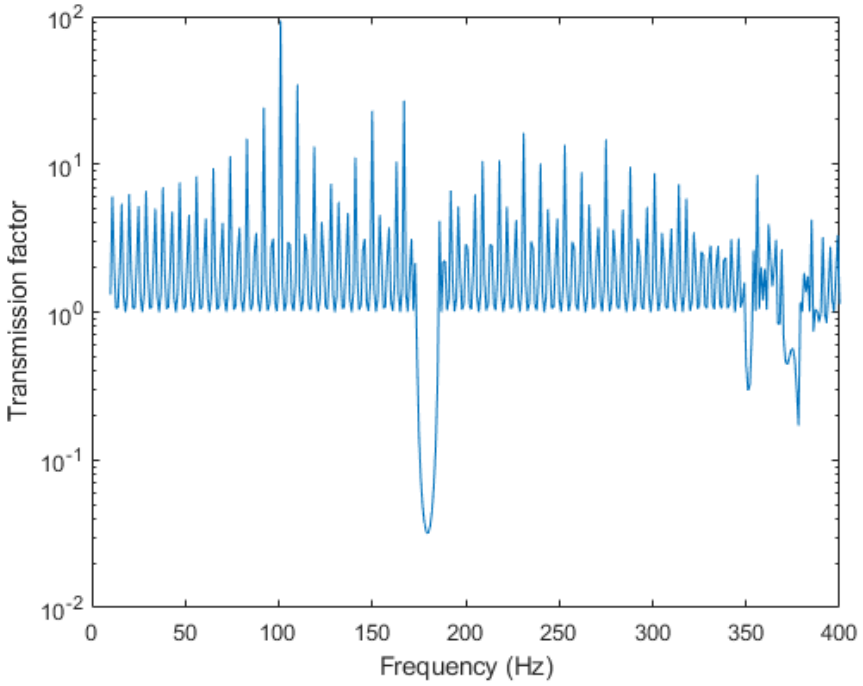

Figure 12: Transmission factor.

along y. The same stop band effect is seen in figure 14 at 350Hz but this time the solution has a more complex variation along y as can be seen in the detail solutions for the substructure $(19, 9)$. As the frequency is higher the difference between the FEM and WFE is larger. Finally, figure 15 is plotted for the frequency 285Hz. As this frequency is in a pass band there is no real attenuation of the solution along x. We show the complexity of the solutions for the substructure $(19, 9)$ at this frequency. The difference between the FEM and WFE is quite low in this case.

Then figures 16 present the modulus of the WFE solutions for a point force excitation located at the middle of the left boundary for frequencies from 20Hz to 1000Hz. The global structure is made of 40×20 substructures. For low frequencies (10Hz to 50Hz), rather classical modes shapes are observed. For medium frequencies (140Hz to 350Hz), the influence of substructures can be clearly seen and complex mode shapes are found. For high frequencies (500Hz and 1000Hz), a more uniform pattern is observed. Finally, figures 17 and 18 present the solutions at 50Hz and 180Hz for a 200×100 structure. To allow a comparison with FEM results, the mesh density was reduced by decreasing the number of nodes of figure 10 by a factor 2.5 on each side. Otherwise the FEM calculation is too big to run on a personal computer. Complex shapes can be observed at both frequencies with some patterns much larger that the substructures. It can be observed that the difference between the FEM and WFE is still small in these cases.

7. Conclusion

We have developed a new method to compute two-dimensional periodic media for the case of a scalar wave equation. This is based on the Wave Finite Element Method by considering propagation along the two directions parallel to the boundary of a substructure. The hypothesis of a symmetric structure and building wave modes with null forces on half of the boundary allow to solve the problem by FFT, leading to a decoupling of all waves and the solutions of many very small systems which is much more efficient than the solution of a large global system. The computating time is considerably

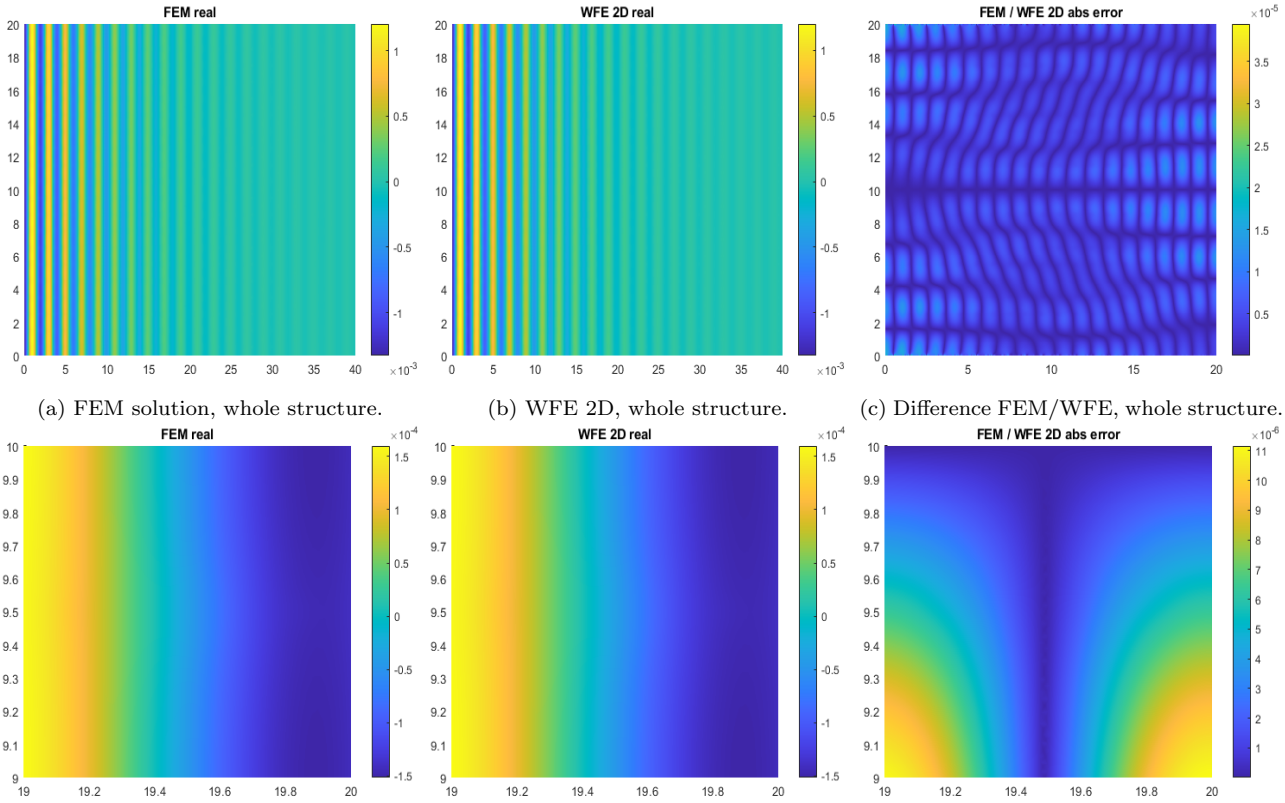

(a) FEM solution, whole structure. (b) WFE 2D, whole structure. (c) Difference FEM/WFE, whole structure.

(d) FEM solution, cell (19,9). (e) WFE 2D, cell (19,9). (f) Difference FEM/WFE, cell (19,9).

Figure 13: Comparison of the FEM and WFE 2D solutions at 180Hz for a uniform excitation on the left boundary.

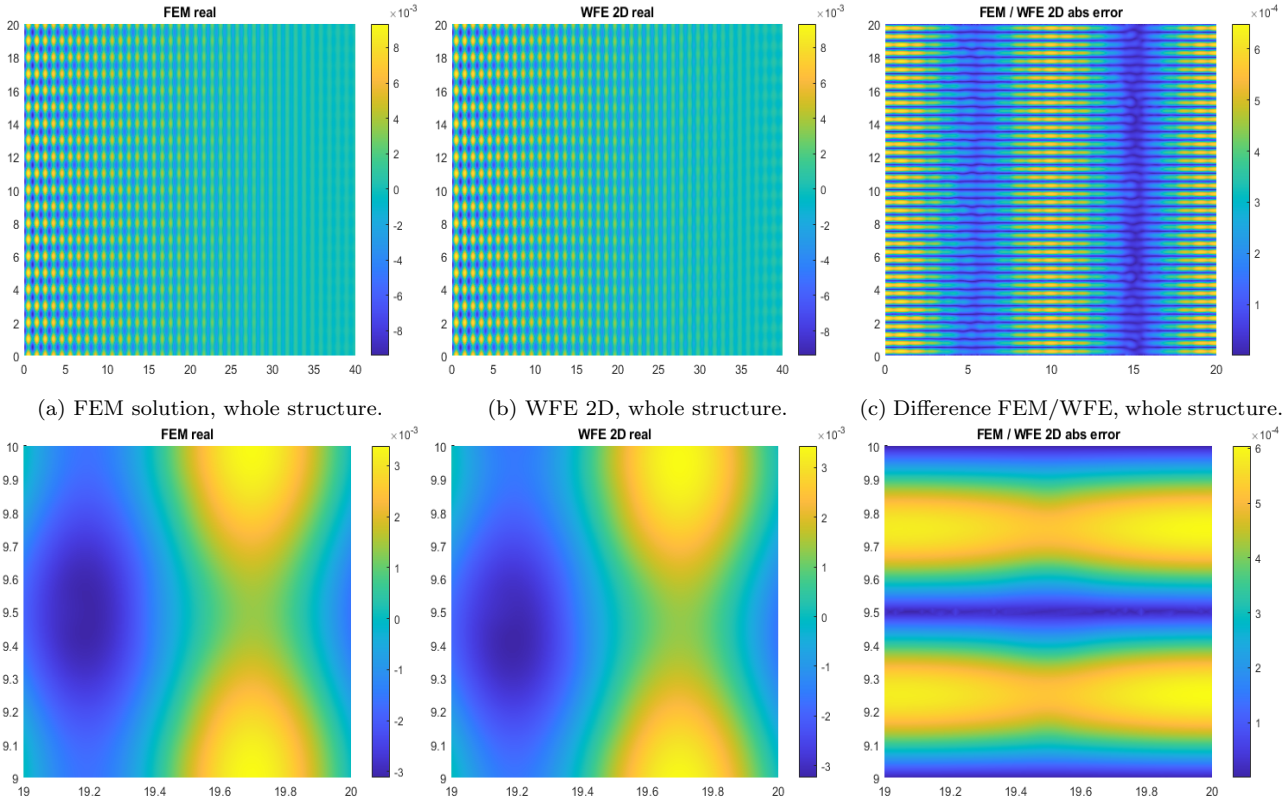

(a) FEM solution, whole structure. (b) WFE 2D, whole structure. (c) Difference FEM/WFE, whole structure.

(d) FEM solution, cell (19,9). (e) WFE 2D solution, cell (19,9). (f) Difference FEM/WFE, cell (19,9).

Figure 14: Comparison of the FEM and WFE 2D solutions at 350Hz for a uniform excitation on the left boundary.

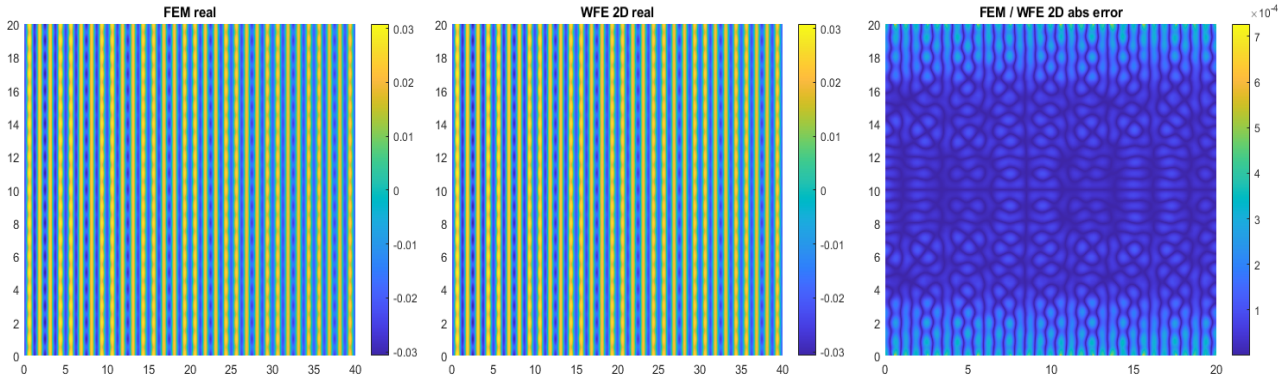

(a) FEM solution, whole structure. (b) WFE 2D, whole structure. (c) Difference FEM/WFE, whole structure.

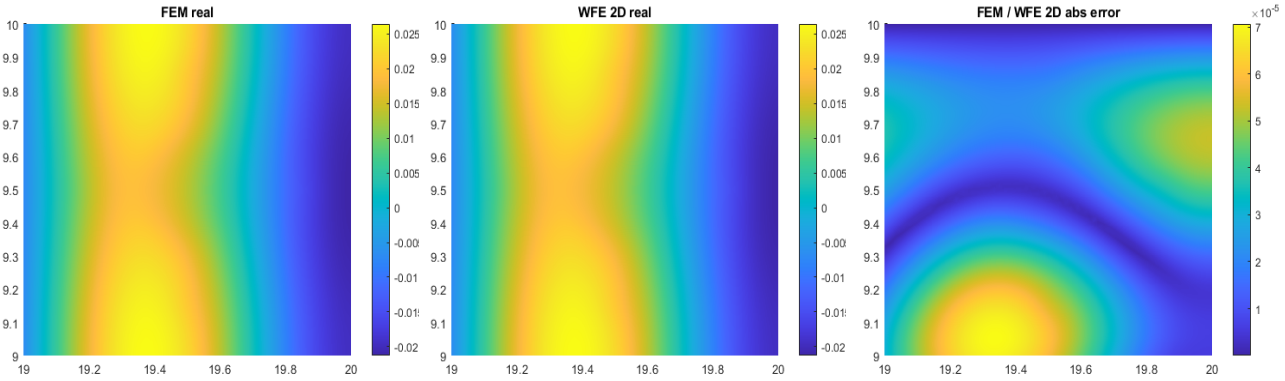

(d) FEM solution, cell (19,9). (e) WFE 2D, cell (19,9). (f) Difference FEM/WFE, cell (19,9).

Figure 15: Comparison of the FEM and WFE 2D solutions at 285Hz for a uniform excitation on the left boundary.

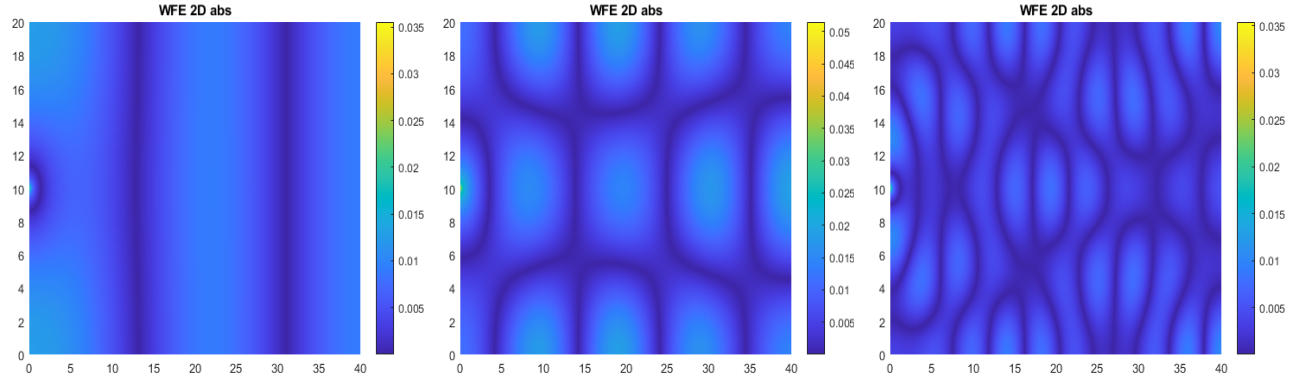

(a) WFE 2D solution at 10Hz.

(b) WFE 2D solution at 25Hz.

(c) WFE 2D solution at 50Hz.

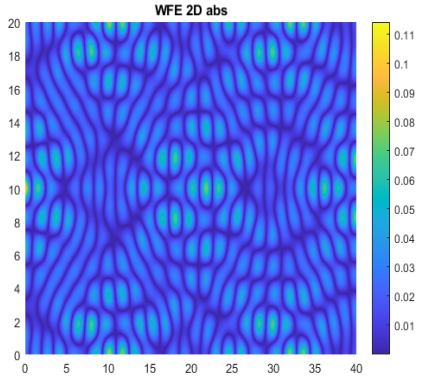

(d) WFE 2D solution at 140Hz.

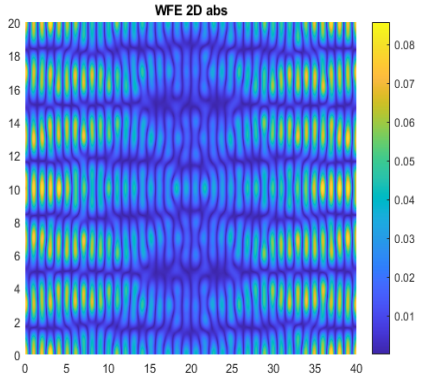

(e) WFE 2D solution at 180Hz.

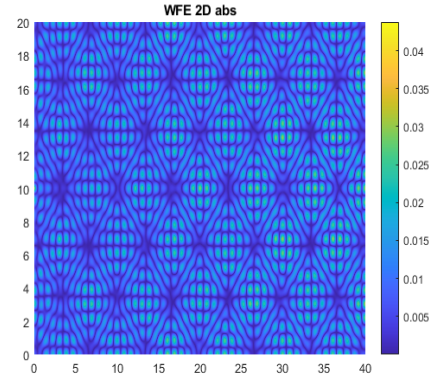

(f) WFE 2D solution at 285Hz.

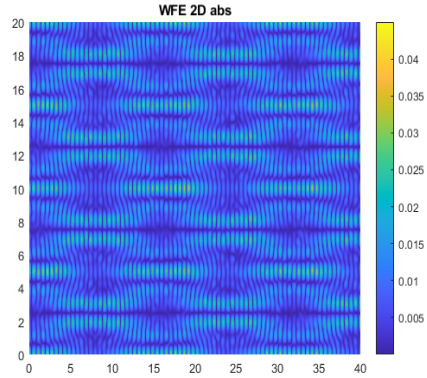

(g) WFE 2D solution at 350Hz.

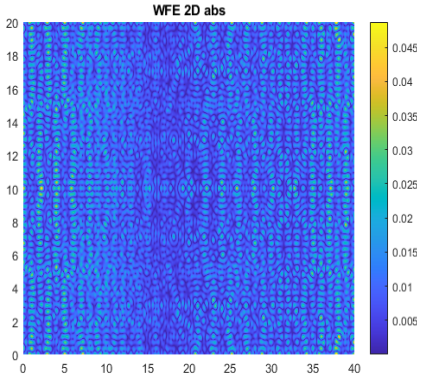

(h) WFE 2D solution at 500Hz.

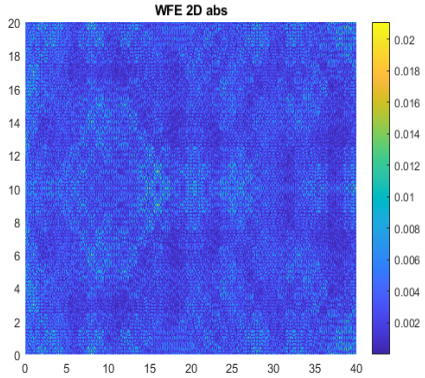

(i) WFE 2D solution at 1000Hz.

Figure 16: Modulus of the WFE 2D solution at different frequencies for a point force excitation in the middle of the left boundary.

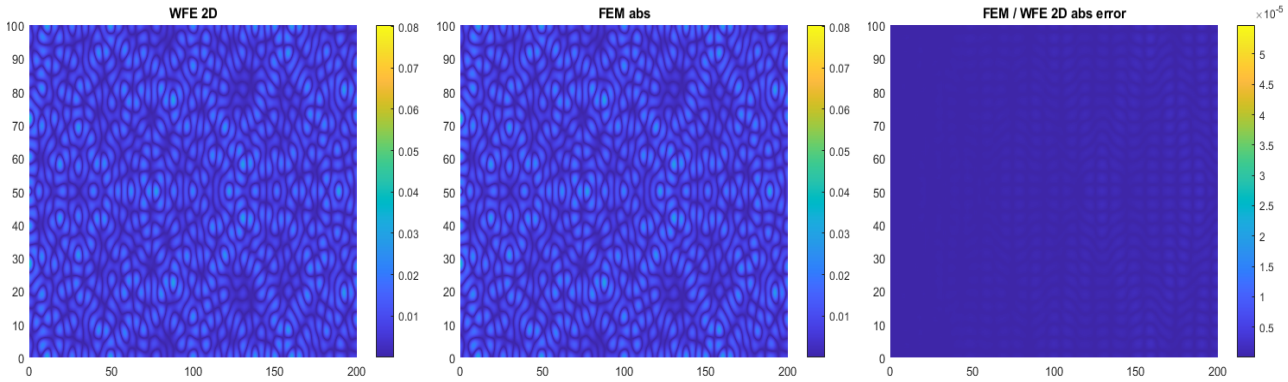

(a) WFE 2D solution. (b) FEM solution. (c) Modulus of the difference FEM/WFE.

Figure 17: Modulus of the solution at 50Hz for a 200×100 structure.

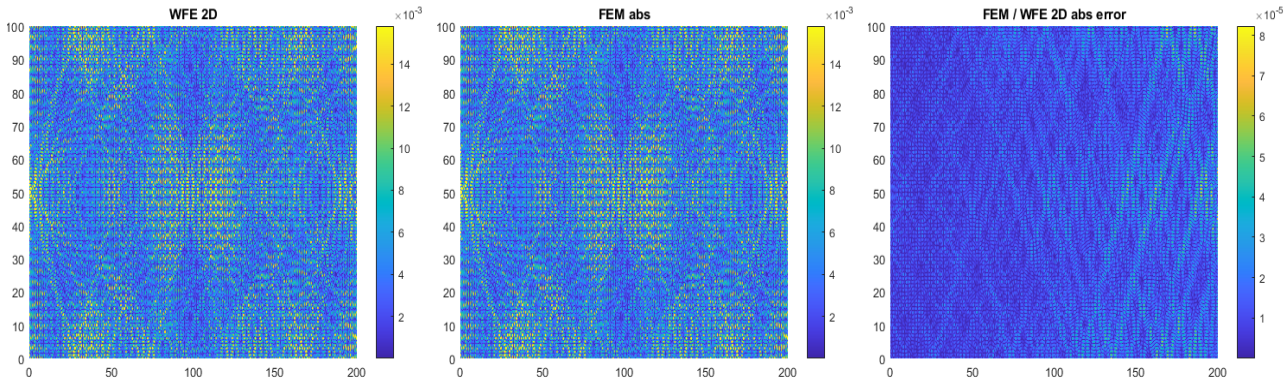

(a) WFE 2D solution. (b) FEM solution. (c) Modulus of the difference FEM/WFE.

Figure 18: Modulus of the solution at 180Hz for a 200×100 structure.

shorter than for a conventional finite element calculation, and the memory requirements remain very low. For a boundary excitation, the method proves to be very efficient and allows to get the solution for structures made of millions of substructures. Results shows complex spatial shapes of the solutions and strong variations with the frequency. In future works, the use of the Green's function of the periodic medium could make it possible to consider the case of loadings inside the domain. We should also try to extend the method for the case of two-dimensional elasticity, meaning structures described by vectorial equations and substructures having no special symmetry. For instance, the case of elasticity requires a more detailed study of the symmetry because the displacement vector has components that react differently to a plane symmetry.

Acknowledgement

The author would like to thank the anonymous referees who provided many useful and detailed comments on the manuscript which greatly improved its readability.

References

[1] B. Mace, D. Duhamel, M. Brennan, L. Hinke, Finite element prediction of wave motion in structural waveguides, Journal of the Acoustical Society of America 117 (2005) 2835–2843. doi:https://doi.org/10.1121/1.1887126.

[2] D. Duhamel, B. R. Mace, M. J. Brennan, Finite element analysis of the vibrations of waveguides and periodic structures, Journal of Sound and Vibration 294 (1-2) (2006) 205–220. doi:https://doi.org/10.1016/j.jsv.2005.11.014.

[3] J.-M. Mencik, D. Duhamel, A wave-based model reduction technique for the description of the dynamic behavior of periodic structures involving arbitrary-shaped substructures and large-sized finite element models, Finite Elements in Analysis and Design 101 (2015) 1–14. doi:https://doi.org/10.1016/j.finel.2015.03.003.

[4] J.-M. Mencik, M. N. Ichchou, Multi-mode propagation and diffusion in structures through finite elements, European Journal of Mechanics - A/Solids 24 (5) (2005) 877–898. doi:https://doi.org/10.1016/j.euromechsol.2005.05.004.

[5] J.-M. Mencik, D. Duhamel, A wave finite element-based approach for the modeling of periodic structures with local perturbations, Finite Elements in Analysis and Design 121 (2016) 40–51. doi:https://doi.org/10.1016/j.finel.2016.07.010.

[6] J.-M. Mencik, New advances in the forced response computation of periodic structures using the wave finite element (WFE) method, Computational Mechanics 54 (3) (2014) 789–801. doi:https://doi.org/10.1007/s00466-014-1033-1.

[7] J.-M. Mencik, A model reduction strategy for computing the forced response of elastic waveguides using the wave finite element method, Computer Methods in Applied Mechanics and Engineering 229-232 (2012) 68–86. doi:https://doi.org/10.1016/j.cma.2012.03.024.

[8] J.-M. Mencik, A wave finite element approach for the analysis of periodic structures with cyclic symmetry in dynamic substructuring, Journal of Sound and Vibration 431 (2018) 441–457. doi:https://doi.org/10.1016/j.jsv.2018.05.027.

[9] M. N. Ichchou, J.-M. Mencik, W. J. Zhou, Wave finite elements for low and mid-frequency description of coupled structures with damage, Computer Methods in Applied Mechanics and Engineering 198 (15-16) (2009) 1311–1326. doi:https://doi.org/10.1016/j.cma.2008.11.024.

[10] T. Hoang, D. Duhamel, G. Foret, Wave finite element method for waveguides and periodic structures subjected to arbitrary loads, Finite Elements in Analysis and Design 179 (2020) 103437. doi:https://doi.org/10.1016/j.finel.2020.103437.

[11] J. M. Renno, B. R. Mace, On the forced response of waveguides using the wave and finite element method, Journal of Sound and Vibration 329 (26) (2010) 5474–5488. doi:https://doi.org/10.1016/j.jsv.2010.07.009.

[12] Y. Waki, B. Mace, M. Brennan, Free and forced vibrations of a tyre using a wave/finite element approach, Journal of Sound and Vibration 323 (3) (2009) 737–756. doi:https://doi.org/10.1016/j.jsv.2009.01.006.

[13] R. Singh, C. Droz, M. Ichchou, F. Franco, O. Bareille, S. De Rosa, Stochastic wave finite element quadratic formulation for periodic media: 1D and 2D, Mechanical Systems and Signal Processing 136 (2020) 106431. doi:https://doi.org/10.1016/j.ymssp.2019.106431.

[14] Y. Fan, C. W. Zhou, J. P. Laine, M. Ichchou, L. Li, Model reduction schemes for the wave and finite element method using the free modes of a unit cell, Computers & Structures 197 (2018) 42–57. doi:https://doi.org/10.1016/j.compstruc.2017.11.015.

[15] A. Abdel-Rahman, Matrix analysis of wave propagation in periodic systems, Ph.D. thesis, University of Southampton (1979).

[16] R. S. Langley, A note on the force boundary conditions for two-dimensional periodic structures with corner freedoms, Journal of Sound and Vibration 167 (2) (1993) 377–381. doi:https://doi.org/10.1006/jsvi.1993.1341.

[17] A. S. Phani, J. Woodhouse, N. A. Fleck, Wave propagation in two-dimensional periodic lattices, The Journal of the Acoustical Society of America 119 (4) (2006) 1995–2005. doi:10.1121/1.2179748.

[18] E. Manconi, Modelling wave propagation in two–dimensional structures using a wave/finite element technique, Ph.D. thesis, University of Parma (2008).

[19] C. W. Zhou, J. P. Lainé, M. N. Ichchou, A. M. Zine, Multi-scale modelling for two-dimensional periodic structures using a combined mode/wave based approach, Computers & Structures 154 (2015) 145–162. doi:https://doi.org/10.1016/j.compstruc.2015.03.006.

[20] A. Palermo, A. Marzani, Extended Bloch mode synthesis: Ultrafast method for the computation of complex band structures in phononic media, International Journal of Solids and Structures 100-101 (2016) 29–40. doi:https://doi.org/10.1016/j.ijsolstr.2016.06.033.

[21] A. Aladwani, M. Nouh, M. I. Hussein, State-space Bloch mode synthesis for fast band-structure calculations of non-classically damped phononic materials, Computer Methods in Applied Mechanics and Engineering 396 (2022) 115018. doi:https://doi.org/10.1016/j.cma.2022.115018.

[22] D. Krattiger, M. I. Hussein, Bloch mode synthesis: Ultrafast methodology for elastic band-structure calculations, Phys. Rev. E 90 (2014) 063306. doi:https://doi.org/10.1103/PhysRevE.90.063306.

[23] C. Droz, C. Zhou, M. N. Ichchou, J.-P. Lainé, A hybrid wave-mode formulation for the vibroacoustic analysis of 2D periodic structures, Journal of Sound and Vibration 363 (2016) 285–302. doi:https://doi.org/10.1016/j.jsv.2015.11.003.

[24] D. Krattiger, M. I. Hussein, Generalized Bloch mode synthesis for accelerated calculation of elastic band structures, Journal of Computational Physics 357 (2018) 183–205. doi:https://doi.org/10.1016/j.jcp.2017.12.016.

[25] L. Van Belle, N. G. R. de Melo Filho, M. Clasing Villanueva, C. Claeys, E. Deckers, F. Naets, W. Desmet, Fast metamaterial design optimization using reduced order unit cell modeling, in: International Conference on Noise and Vibration Engineering (ISMA 2020), Leuven, Belgium, 7-9 September, 2020, pp. 2487–2502.

[26] M. I. Hussein, Reduced Bloch mode expansion for periodic media band structure calculations, Proc. R. Soc. A. 465 (2009) 2825–2848. doi:https://doi.org/10.1098/rspa.2008.0471.

[27] M. J. Leamy, Exact wave-based Bloch analysis procedure for investigating wave propagation in two-dimensional periodic lattices, Journal of Sound and Vibration 331 (7) (2012) 1580–1596. doi:https://doi.org/10.1016/j.jsv.2011.11.023.

[28] M. Collet, M. Ouisse, M. Ruzzene, M. N. Ichchou, Floquet–Bloch decomposition for the computation of dispersion of two-dimensional periodic, damped mechanical systems, International Journal of Solids and Structures 48 (20) (2011) 2837–2848. doi:https://doi.org/10.1016/j.ijsolstr.2011.06.002.

[29] V. Thierry, L. Brown, D. Chronopoulos, Multi-scale wave propagation modelling for two-dimensional periodic textile composites, Composites Part B: Engineering 150 (2018) 144–156. doi:https://doi.org/10.1016/j.compositesb.2018.05.052.

[30] B. R. Mace, E. Manconi, Modelling wave propagation in two-dimensional structures using finite element analysis, Journal of Sound and Vibration 318 (4-5) (2008) 884–902. doi:https://doi.org/10.1016/j.jsv.2008.04.039.

[31] J. M. Renno, B. R. Mace, Vibration modelling of helical springs with non-uniform ends, Journal of Sound and Vibration 331 (12) (2012) 2809–2823. doi:https://doi.org/10.1016/j.jsv.2012.01.036.

[32] C. W. Zhou, F. Treyssède, Two-dimensional elastic Bloch waves in helical periodic structures, International Journal of Solids and Structures 204-205 (2020) 34–51. doi:https://doi.org/10.1016/j.ijsolstr.2020.06.026.

[33] J. Renno, S. Sassi, S. Gowid, Wave propagation in double helical rods, Wave Motion 93 (2020) 102446. doi:https://doi.org/10.1016/j.wavemoti.2019.102446.

[34] Q. Wei, X. Ma, J. Xiang, Band structure analysis of two-dimensional photonic crystals using the wavelet-based boundary element method, Engineering Analysis with Boundary Elements 134 (2022) 1–10. doi:https://doi.org/10.1016/j.enganabound.2021.09.025.

[35] F. Maurin, Bloch theorem with revised boundary conditions applied to glide and screw symmetric, quasi-one-dimensional structures, Wave Motion 61 (2016) 20–39. doi:https://doi.org/10.1016/j.wavemoti.2015.10.008.

[36] F. Maurin, C. Claeys, L. Van Belle, W. Desmet, Bloch theorem with revised boundary conditions applied to glide, screw and rotational symmetric structures, Computer Methods in Applied Mechanics and Engineering 318 (2017) 497–513. doi:https://doi.org/10.1016/j.cma.2017.01.034.

[37] T. F. Eibert, J. L. Volakis, D. R. Wilton, D. R. Jackson, Hybrid FE/BI modeling of 3-D doubly periodic structures utilizing triangular prismatic elements and an MPIE formulation accelerated by the Ewald transformation, IEEE Transactions on Antennas and Propagation 47 (5) (1999). doi:10.1109/8.774139.

[38] D. Duhamel, Finite element computation of Green's functions, Engineering Analysis with Boundary Elements 31 (11) (2007) 919–930. doi:https://doi.org/10.1016/j.enganabound.2007.04.002.

[39] J. M. Renno, B. R. Mace, Calculating the forced response of two-dimensional homogeneous media using the wave and finite element method, Journal of Sound and Vibration 330 (24) (2011) 5913–5927. doi:https://doi.org/10.1016/j.jsv.2011.06.011.

[40] J.-F. Lu, J. Cheng, Q.-S. Feng, Plane wave finite element model for the 2-D phononic crystal under force loadings, European Journal of Mechanics - A/Solids 91 (2022) 104426. doi:https://doi.org/10.1016/j.euromechsol.2021.104426.

[41] R. S. Langley, The response of two-dimensional periodic structures to point harmonic forcing, Journal of Sound and Vibration 197 (4) (1996) 447–469. doi:https://doi.org/10.1006/jsvi.1996.0542.

[42] R. S. Langley, The response of two-dimensional periodic structures to impulsive point loading, Journal of Sound and Vibration 201 (2) (1997) 235–253. doi:https://doi.org/10.1006/jsvi.1996.0744.

[43] J. A. Kulpe, K. G. Sabra, M. J. Leamy, Bloch-wave expansion technique for predicting wave reflection and transmission in two-dimensional phononic crystals, The Journal of the Acoustical Society of America 135 (4) (2014) 1808–1819. doi:10.1121/1.4864457.

[44] C. Dong, Effective elastic properties of doubly periodic array of inclusions of various shapes by the boundary element method, International Journal of Solids and Structures 43 (2006) 7919–7938. doi:https://doi.org/10.1016/j.ijsolstr.2006.04.009.

[45] Y. Yan, A. Laskar, Z. Cheng, F. Menq, Y. Tang, Y. L. Mo, Z. Shi, Seismic isolation of two dimensional periodic foundations, Journal of Applied Physics 116 (4) (2014) 044908. doi:https://doi.org/10.1063/1.4891837.

[46] I. Andonegui, A. J. Garcia-Adeva, The finite element method applied to the study of two-dimensional photonic crystals and resonant cavities, Optics Express 21 (4) (2013) 4072–4092. doi:10.1364/OE.21.004072.

[47] J.-M. Mencik, M.-L. Gobert, Acoustic radiation of 2D nearly periodic metamaterial plates via finite element procedures and model reduction strategies, in: International Conference on Noise and Vibration Engineering (ISMA 2022), Leuven, Belgium, 12-14 Sep., 2022, pp. 3013–3022.

[48] L. Van Belle, C. Claeys, E. Deckers, W. Desmet, Fast forced response calculations of finite metamaterial plates using a generalized Bloch mode synthesis based sub-structuring approach, in: Proceedings of Euronoise, Madeira, Portugal, 25-27 October, 2021, pp. 1–10.

[49] F. Qu, L. Van Belle, E. Deckers, A unit cell wave based reduced order modelling approach for fast vibration response calculations of finite periodic metamaterial plates, in: International Conference on Noise and Vibration Engineering (ISMA 2022), Leuven, Belgium, 12-14 Sep., 2022, pp. 3133–3147.

[50] S. van Ophem, E. Deckers, W. Desmet, Efficient assembly of unit cells with Krylov based model order reduction, in: International Conference on Noise and Vibration Engineering (ISMA 2018), Leuven, Belgium, 17-19 September, 2018, pp. 445–456.

[51] M. Shadi Mohamed, M. Seaid, J. Trevelyan, O. Laghrouche, A partition of unity FEM for time-dependent diffusion problems using multiple enrichment functions, International Journal for Numerical Methods in Engineering 93 (3) (2013) 245–265. doi:https://doi.org/10.1002/nme.4383.

[52] M. S. Mohamed, O. Laghrouche, J. Trevelyan, A q-adaptive partition of unity finite element method for the solution of the 2-D helmholtz equation, IOP Conference Series: Materials Science and Engineering 10 (1) (2010) 012148. doi:10.1088/1757-899X/10/1/012148.

[53] M. Malek, N. Izem, M. Seaid, M. S. Mohamed, M. Wakrim, A partition of unity finite element method for nonlinear transient diffusion problems in heterogeneous materials, Computational and Applied Mathematics 38 (2) (2019) 31. doi:10.1007/s40314-019-0782-z.

[54] M. Malek, N. Izem, M. S. Mohamed, M. Seaid, O. Laghrouche, A partition of unity finite element method for three-dimensional transient diffusion problems with sharp gradients, Journal of Computational Physics 396 (2019) 702–717. doi:https://doi.org/10.1016/j.jcp.2019.06.062.

[55] M. Iqbal, H. Gimperlein, O. Laghrouche, K. Alam, M. Shadi Mohamed, M. Abid, A residual a posteriori error estimate for partition of unity finite elements for three-dimensional transient heat diffusion problems using multiple global enrichment functions, International Journal for Numerical Methods in Engineering 121 (12) (2020) 2727–2746. doi:https://doi.org/10.1002/nme.6328.

[56] A. E. Kahoui, M. Malek, N. Izem, M. S. Mohamed, M. Seaid, Partition of unity finite element analysis of nonlinear transient diffusion problems using p-version refinement, Computer Modeling in Engineering & Sciences 124 (1) (2020) 61–78. doi:10.32604/cmes.2020.010874.

[57] G. Tanner, Dynamical energy analysis—Determining wave energy distributions in vibro-acoustical structures in the high-frequency regime, Journal of Sound and Vibration 320 (4) (2009) 1023–1038. doi:https://doi.org/10.1016/j.jsv.2008.08.032.

[58] D. J. Chappell, S. Giani, G. Tanner, Dynamical energy analysis for built-up acoustic systems at high frequencies, The Journal of the Acoustical Society of America 130 (3) (2011) 1420–1429. doi:https://10.1121/1.3621041.

[59] D. J. Chappell, G. Tanner, S. Giani, Boundary element dynamical energy analysis: A versatile method for solving two or three dimensional wave problems in the high frequency limit, Journal of Computational Physics 231 (18) (2012) 6181–6191. doi:https://doi.org/10.1016/j.jcp.2012.05.028.